Analysis of the Thermodynamics and Dynamics of Tropical Mesoscale Convective Systems

Rebecca L. Mangini-Hall

A Thesis submitted in partial fulfillment of

the requirements for the degree of

Master of Science

(Atmospheric and Oceanic Sciences)

at the

University of Wisconsin-Madison

December 2024

Thesis Declaration and Approval

I, Rebecca L. Mangini-Hall, declare that this Thesis titled 'Analysis of the Thermodynamics and Dynamics of Tropical Mesoscale Convective Systems' and the work presented in it are my own.

Rebecca L. Mangini-Hall		
Author	Signature	Date

I hereby approve and recommend for acceptance this work in partial fulfillment of the requirements for the degree of Master of Science:

Ángel F. Adames Corraliza		
Committee Chair	Signature	Date

Angela Rowe		
Faculty Member	Signature	Date

Larissa Back		
Faculty Member	Signature	Date

Abstract

Analysis of the Thermodynamics and Dynamics of Tropical Mesoscale Convective Systems

by Rebecca L. Mangini-Hall

Satellite data combined with a reanalysis product is used to identify the thermodynamic and dynamic controls that govern mesoscale convective systems (MCSs). Composites are made of MCSs occurring within the tropics (30^{o}S to 30^{o}N) during 2014-2016, excluding those associated with tropical cyclones. The life of an MCS is divided into three stages: growth or initiation, maturity, and decay. Stage 1 shows divergence near 500 hPa that is characterized by warm and dry anomalies, indicative of a stable layer that caps convection. Stage 2 is distinguished from the other life cycle phases in exhibiting a cooler and moister lower troposphere. The third stage exhibits convergence in the mid-troposphere and further aloft at the tropopause, indicative of anvil remnants. Results show large accumulations of lower tropospheric moisture and instability are linked to the buoyancy and vertical motion that large-scale precipitation requires. A temporal gap is observed between greatest plume buoyancy and moisture/precipitation through the MCS life cycle. Buoyancy is a maximum in stage 1, while rainfall is a maximum in stage 2, a time when buoyancy is near zero. The near-zero buoyancy is due to a cancellation between instability and dilution. During stage 3, decay is associated with the stabilization of the lower troposphere and the cessation of convection.

”Lo duca e io per quel cammino ascoso
intrammo a ritornar nel chiaro mondo;
e sanza cura aver dálcun riposo,
salimmo sú, el primo e io secondo,
tanto ch’i’ vidi de le cose belle
che porta ’l ciel, per un pertugio tondo.
E quindi uscimmo a riveder le stelle.”

Dante Alighieri, Inferno

This work is dedicated to all women in atmospheric science.
May we find the answers we seek.

Acknowledgements

First, I would like to thank my advisor, Professor Ángel F. Adames-Corraliza, for all of his help and patience the past 2 and a half years. Through many difficult times, your unwavering support and faith meant a lot to me.

My committee, Professors Larissa Back and Angela Rowe, for their wisdom and guidance; I'm so appreciative for all the advice!

A huge thank you to all the professors and administrators (and Pete) in the department for your knowledge, aid, and patience.

-

So, so, so many thanks to all of the wonderful friends I've made here in Madison:

Ruby- you were my first friend in the department and I'm so incredibly grateful for your friendship (even if you're no longer here #gonebutnotforgotten).

Rosa and Victor- thank you so much for your friendship and support through both the good and the bad times.

Jack- you were not directly mentioned in my diary, but I hope this makes up for that: you're a great friend and I'm very grateful that our paths have crossed.

Karissa and Abbi- Lesbian pop-up bars were a lot of fun and so validating, thank you!

Libby, Patrick, and Flora- thank you so much for granting me a space outside of my office to both procrastinate and vent. (also, thank you to Patrick for lending his colorblindness -xoxo)

Grant- I think our ability to get under each other's skin is a symptom of how similar we are and I'm actually very thankful for the solidarity. You've made me want to strive to be both a better person and friend; your impact on my life has been profound, thank you.

Carolyn- to a fellow band nerd and victim of 2014 tumblr: thank you for your stories and camaraderie!

To my roommates: Autumn, Tanner, Binx, and Lady- I love all of y'all and I'd like to specifically thank you for providing listening ears and reassurance through it all.

-

To my friends from home: Lyren, Alaina, and Carl- I can't even begin to express how thankful I am for all your love and support. Following my passion for clouds wouldn't have happened without your encouragement. I hope to be able to one day return even a fraction of what y'all have done for me.

-

To my family: thank you so so much, none of this would have been possible without you.
Mom- you're a pillar in my life and I aspire to be as strong and resilient as you.
Dad- you showed me the music present in living, something I hold onto when the days seem dark (and I attribute my passion for science to all the Star Trek, Star Wars, Eureka!, and Myth Busters we watched as I grew up).
To both of you and Matches: thank you and SHMILY

-

Many thanks to the developers and maintainers of the TIMPS storm tracking database, a crucial piece to our research puzzle.
I'd additionally like to thank the National Defense Science and Engineering Graduate Fellowship and the National Science Foundation's award #2225955 for their support in conducting the research presented here.

Contents

Abstract **ii**

Dedication **iv**

Acknowledgements **v**

Contents **vii**

List of Figures **ix**

List of Tables **x**

1 Introduction **1**
1.1 The Mesoscale Convective System 1
1.2 Associated Historical and Contemporary Research 5
1.3 The Research Question & Main Hypotheses 8

2 Data and Methods **11**
2.1 IMERG 11
2.2 ERA5 12
2.3 TIMPS 12
2.4 Storm-Centered Composites 15
2.5 Plume Buoyancy 15

3 Analysis of Data Selection Validity **18**
3.1 Moist Thermodynamic State 18
3.2 Precipitation in Reanalysis and Satellite Data 21

4 Environmental Thermodynamics and Circulation Features **26**
4.1 Vertical Motion 26
4.2 Vertical Structure Changes 28

5 Plume Buoyancy **36**
5.1 Evolution of Plume Buoyancy in the MCS Life Cycle 36

5.2 Full Plume Profile of Convective Instability & Vertical Motions 39

6 Summary & Conclusions **42**

6.1 Addressing the Hypotheses 42

6.2 Stipulations in Using ERA5 Data 48

6.3 Future Plans and Applications 50

6.4 An Afterword 51

List of Figures

1.1 Precipitation Climatology 2
1.2 The MCS Life Cycle 4
1.3 Entrainment Schematic 8

3.1 Storm Density and Total Column Water Vapor 19
3.2 Barplots of Thermodynamic Variables 20
3.3 Composite of Column-Integrated Thermodynamic Variables 22
3.4 Areal Composite Comparison of Precipitation Data 23
3.5 ERA5 vs. IMERG Precipitation Data 24
3.6 ERA5 Precipitation vs. Vertical Velocity 25

4.1 Areal Composites of Omega at Different Pressure Levels 28
4.2 Vertical Omega Profiles 29
4.3 Vertical Temperature Profiles 31
4.4 Vertical Temperature Profiles: Stage Differences 32
4.5 Vertical Specific Humidity Profiles 33
4.6 Vertical Specific Humidity Profiles: Stage Differences 34

5.1 Decomposed Plume Buoyancy 38
5.2 Vertical MSE and Omega Profiles 40

6.1 Schematic of Results 44

List of Tables

2.1 Used Variables 13

Chapter 1

Introduction

1.1 The Mesoscale Convective System

The highest rainfall rates on the planet occur in the tropics (Figure 1.1), where nearly 93% of the annual precipitation observed is a result of organized deep convection events known as mesoscale convective systems (MCS) (Houze Jr, 2004, Roca and Fiolleau, 2020). They are broadly defined as a collection of storms larger than a single thunderstorm but smaller than an extratropical cyclone; they include phenomena such as squall lines and mesoscale convective complexes. These systems play a pivotal role in our planet's weather and climate. They contain large anvil and cirrus cloud decks that impact the global radiation budget via reflection of short-wave radiation as well as absorption of long-wave radiation (Rajagopal et al., 2023). Constituted by both convective and stratiform rain regions, these systems serve as ideal setups to conduct analysis on convection and its

ties to the surrounding environmental influences. Relationships between deep convection and the surrounding environment remain uncertain, where questions persist regarding their governing forces including those responsible for the occurrence and organization of tropical rainfall.

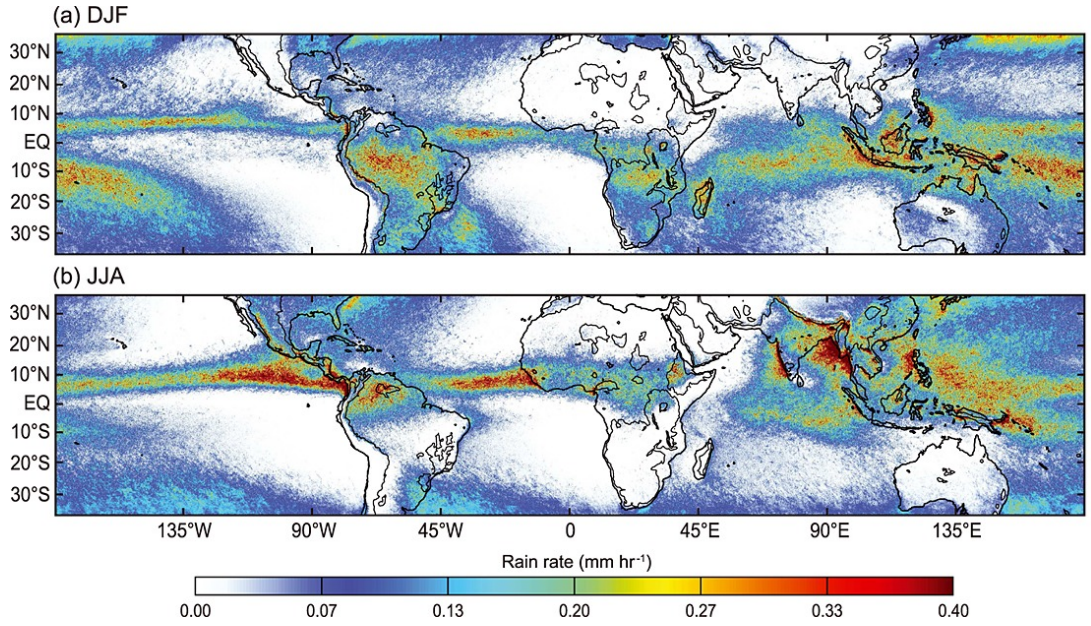

FIGURE 1.1: Precipitation climatology expressed in average rain rates (mmhr^{-1}) from all TRMM Distinguishable Rain Areas (DRAs) during the months of (a) DJF and (b) JJA from 1998 to 2013. The black contour inside the continental regions represents the 700 m elevation. From Houze et al. 2015.

The tropical deep convection occurring within MCSs is a current point of contention in the realm of tropical meteorology. As a reference to the collective vertical movement of mass and energy within the tropical troposphere, this process, which is vital to Earth's general circulation and redistribution of heat and moisture, has yet to be fully understood. Via their convective and stratiform components, MCSs influence the large-scale tropical circulation and its variability within different time scales (Schumacher et al., 2004). MCSs

also produce and maintain a significant amount of the convective towers that are thought to play a key role in poleward energy transport, establishing them as relevant research beds for tropical convection controls and evolution (Liu et al., 2021, Rajagopal et al., 2023, Riehl and Malkus, 1958).

Neglecting an MCS's life cycle stage may lead to misunderstandings in regards to the true nature of convection's driving forces. Without the context of the system's age and developmental stage, issues can arise in accurately capturing and analyzing the true drivers and impacts of convective growth. To address and prevent such issues, the conducted research focuses on separating the MCSs into three component life cycle stages, as they are outlined in Houze Jr (2004). Figure 1.2 illustrates the key features expected in each life cycle stage.

Stage 1 is characterized by convection initiation and growth where surface wind tendencies are convergent indicating upward movement. Within this premature state, divergence is expected in the middle free troposphere as parcels lack the necessary buoyancy to travel to the upper troposphere. Anticipated cloud morphologies include low and mid-level cumulus species building up to form a mature anvil head. These morphological developments mark an essential component of stage 1: new convective cells (i.e. immature cumulus) form and grow at a rate faster than the dissipation time of older cell decay (Houze Jr, 2004).

Stage 2 is the period where MCSs reach maturity. Quantitatively, this is when the system reaches its maximum size and precipitation output. New convective cores are

growing at the same rate in which older cores dissipate into the stratiform deck (Houze Jr, 2004). Surface wind tendencies converge as active deep convection occurs throughout the tropospheric column and flow diverges at its top.

Lastly, stage 3 is the period of convective decay. Heralding the end of new convective core creation, it's characterized by shrinking areal extent and decreasing volumetric rain rates. Stratiform regions precipitate out faster than new convective cores can develop (Houze Jr, 2004). Surface wind tendencies are expected to diverge alongside mass precipitation fallout. Cloud morphology includes decaying cumulus, anvil remnants, and the precipitating stratiform deck. While these structures persist, divergent flow is expected at the top of the troposphere, as in stage 2.

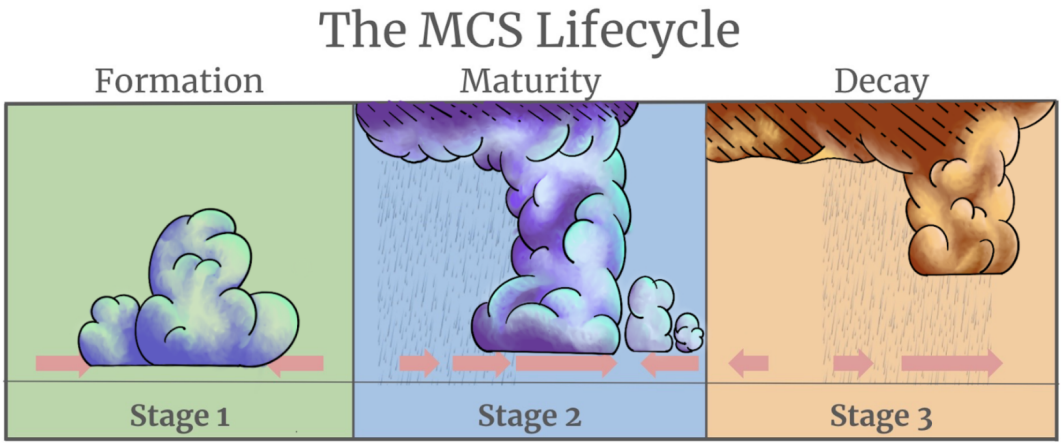

FIGURE 1.2: The MCS lifecycle broken down into its three component parts: stages 1, 2, and 3. Pink arrows indicate surface wind tendencies and expected cloud morphologies are shown.

1.2 Associated Historical and Contemporary Research

The original hot tower hypothesis for tropical convection, posed by Riehl and Malkus (1958), proposed undilute plumes transported mass and energy to the top of the troposphere. Their hypothesis emphasized the need for presence of isolated, undilute convective towers in tropical storms to achieve the observed poleward energy and mass movement. With the advent of field and modeling studies conducted in the 1970s and 1980s, alternative theories arose in regards to the manner in which tropical deep convection can be quantitatively analyzed (Houze Jr, 2004). One fundamental theory, the quasi-equilibrium hypothesis, was first postulated by Arakawa and Schubert (1974). In it, they suggest that moist convection uses potential energy at the rate in which it is provided via larger scale processes. This theory establishes that convection is dependent on the relative humidity of the boundary layer, lower free troposphere (LFT), and middle free troposphere (MFT). As a result, this theory suggests environmental mixing with the convective cores is present, breaking away from the original undilute hot tower hypothesis. Further deviating from the original hot tower hypothesis, Zipser's 2003 paper used data from the Tropical Rainfall Measuring Mission (TRMM) to show undilute convective towers are actually very rare in the tropics. Entrainment is instead proposed as a possible solution to achieve the necessary levels of instability and buoyancy for tropical deep convection to occur (Zipser, 2003).

Following these landmark publications, multiple observational and modeling techniques arose attempting to test the aforementioned theories on the thermodynamics of MCSs

and their associated convective cores. One such technique focused on obtaining the temperature brightness of cloud tops via infrared radiation sensors; however, while helpful in determining the area of the MCS cloud deck, later research showed this technique inaccurately estimated rain rates for shallow deep convection and under anvils/icy cloud sheets (Berg and Stull, 2002, Liu and Moncrieff, 2007, Woodley et al., 1980). Other quantifying methods have yielded study results on storm tracking methods, convection's thermodynamic influences, and the importance of environmental mixing and entrainment. Contemporary research has continued this analysis; Raymond et al. (2015) and Adames (2022), for example, are recent theoretical studies focused on different thermodynamic impacts on convection while Houze Jr et al. (2015) analyzed the observed characteristics of MCSs. Additionally, high levels of buoyancy and low-level moisture have been linked to higher probabilities of both MCSs occurring and broadening of their stratiform regions (Ahmed and Schumacher, 2015, Schiro and Neelin, 2019).

Within contemporary research, new MCS tracking methods have evolved to improve observational data accuracy and precision to better capture the nuanced features of these systems. These include Feng et al. (2021), where infrared measurements of cloud top height were matched to observational precipitation data. This dataset, however, does not follow MCSs that split or merge with other precipitating systems. Acting to limit the types of MCS life cycle evolutions included in their analysis, only isolated MCS that did not interact with other precipitating systems were studied. Another tracking method is outlined in Hayden et al. (2021), where the World Wide Lightning Location Network (WWLLN) was co-located to observational precipitation data to study MCS

structures. This method, though, struggled to accurately distinguish nearby and similarly sized MCSs as separate systems. Analysis on MCS life cycles thus requires a tracking dataset that addresses the complexity in following systems through space and time via the identification of separate systems and their relationships to one another.

In consideration of both the historical and contemporary focuses, theory (Arakawa and Schubert, 1974, Moncrieff and Miller, 1976) and observations (Kingsmill and Houze Jr, 1999, Zipser, 2003) support the idea that MCSs entrain environmental air within a deep layer of the lower troposphere as shown in Figure 1.3. This idea has continued to evolve, where most recently, studies have focused on the buoyant relationships between the boundary layer and LFT. In these relationships, the environmental influences on MCSs' strength, organization, evolution, and occurrence has been considered within the context of an entraining plume (Adames et al., 2021, Ahmed et al., 2020, Ahmed and Neelin, 2018, Schiro et al., 2018, Schiro and Neelin, 2019). In considering that context, research has focused on a quantity quasi-conserved within a plume: moist static energy (MSE). A useful metric in quantifying an air parcel's inherent energy, future improvements to our understanding of buoyancy and convection within the tropics will rely on analyzing MSE within the plume buoyancy framework. Through expanding our understanding on how vertical velocities (ω) are influenced within MCSs' convective updrafts, we focus on current diagnostic theory on the structures of MSE and omega within both convectively enhanced and suppressed periods (Benedict et al., 2014, Hannah and Maloney, 2011, 2014, Inoue and Back, 2015a, Masunaga and L'Ecuyer, 2014, Sobel et al., 2014).

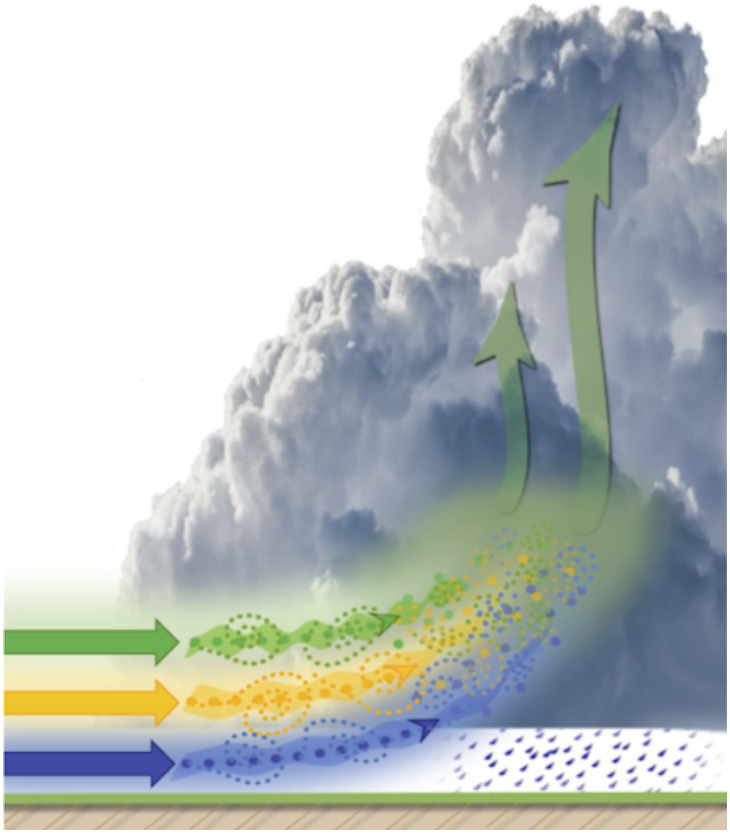

FIGURE 1.3: Schematic of the deep inflow of environmental air into a convecting entity. The inflow can be partly turbulent as has traditionally been assumed for cumulonimbus clouds, and partly coherent as is typical in mesoscale convective systems (12), and is drawn to emphasize the latter. Colors denote an environmental conserved variable entering at different vertical levels at nearly the same rate (Schiro et al., 2018)

1.3 The Research Question & Main Hypotheses

In spite of their importance, the processes that govern tropical MCS growth and decay are not fully understood. For instance, the relationship between deep convection and the surrounding environment in terms of temperature, moisture, and buoyancy is incomplete (Ahmed and Neelin, 2018, Schiro et al., 2018, Schiro and Neelin, 2019). Uncertainties remain in how convective cells evolve and interact with the environment in organized systems, such as MCSs, versus unorganized ones. Attempts at tracking these systems

through time and space in previous research have only followed isolated MCSs and were unable to capture the full lifetimes of systems that merged or split; interactions with other storms were not accounted for. Additionally, parameterizations of convection in current models often see precipitation biases arise from misrepresentation of convective dynamics. In particular, the impact and role of deep-inflow mixing remains uncertain within current models (Schiro and Neelin, 2019). Questions remain in how moist thermodynamics and large-scale dynamics conspire to alter the occurrence and characteristics of MCSs throughout their life cycles. Aspects such as the impact of moisture at different levels of the lower troposphere, entrainment influences on buoyancy, and the relationship between precipitation and buoyancy are persistent unknowns. More specifically, this leads to the main research question motivating this work:

How do buoyancy and moisture affect isolated tropical MCSs throughout their life cycles when considered in an entraining plume framework?

To address the research question, testable hypotheses were posed based upon relevant and recent research. These studies have shown that the occurrence of MCSs is linked to enhanced moisture concentrations in the lower troposphere (Hannah and Maloney, 2011, Holloway and Neelin, 2009, Schiro et al., 2018, Schiro and Neelin, 2019). The first hypothesis of this work is thus an extension of those previous studies: enhanced moisture in the lower troposphere evolves with convection, where maximum column moisture occurs alongside maximum updraft speeds, buoyancy, and precipitation. The second hypothesis extends this idea to convective decay, postulating that updraft dilution by mixing with

the environment acts to suppress buoyancy and is the leading contributor to MCS decay. Stabilization of the boundary layer and LFT is also expected during decay of an MCS. Under this framework, MCS growth is thus anticipated to be constrained via entrainment of dry environmental air in the boundary layer and LFT.

To address our hypotheses, our methodology and data sources are described in section 2. Section 3 justifies the data and storm tracking selections. Results pertaining to bulk environmental thermodynamics and their associated circulation features are covered in section 4. Section 4 helps to contextualize section 5, where application of the plume buoyancy framework is described. Discussions on the results are addressed in the last section alongside the conclusions and future implications.

Chapter 2

Data and Methods

2.1 IMERG

Two different data sets were used to carry out this research. The first is NASA's Integrated Multi-satellite Retrievals for Global Precipitation Measurement (IMERG) V06B Final product (Huffman et al., 2020, 2019). To conduct analysis on precipitation rates and areas, which are relevant to the categorization of MCS life cycle stages, highly-resolved observational data was required. IMERG was chosen as it is an ideal observational dataset that improves upon previous precipitation measuring systems. By utilizing the relationship between infrared cloud features and rain amounts, IMERG ends up with less biases and more reliable data compared to its older counterparts; they instead used features like cloud brightness temperature to quantify precipitation (Feng et al., 2021, Ocasio et al., 2020, Rajagopal et al., 2023). The data is available at 30 minute intervals with

a resolution of 0.1° (Huffman et al., 2020, 2019, Rajagopal et al., 2023). To facilitate comparison with ERA5 data (discussed below), the IMERG data is interpolated to a 0.5° x 0.5° latitude-longitude grid, and to a temporal resolution of 30 minutes.

2.2 ERA5

We also make use of data from the fifth reanalysis product from the European Center for Medium-Range Weather Forecasting (ERA5) to conduct higher resolution analysis of MCSs. This data was chosen due to limited surface observations, especially over the ocean, and gaps present in satellite data. To conduct the necessary research, accurate data on precipitating area and lifetime length of MCSs were needed to analyze the MCS life cycle stages; ERA5 fulfilled this need by having a fine spatial and temporal resolution built from both observations and models. The data used has a fine spatial resolution of 0.5° latitude and longitude and temporal resolution of 6 hours for the 2014-2016 time period. The following field variables are used and summarized in Table 2.1: zonal wind (u), meridional wind (v), vertical pressure velocity (ω), specific humidity (q), temperature (T), equivalent potential temperature (θ), geopotential (Φ), CAPE, CIN, total column water vapor ($< q >$), and precipitation (P).

2.3 TIMPS

The Tracked IMERG Mesoscale Precipitation Systems (Russell, 2021) is used to pick MCS events for compositing. TIMPS utilizes the Forward in Time (FiT) algorithm, which tracks precipitation systems in the IMERG (Huffman et al. 2019) data and does so

	Variable	Units
u, v	Horizontal Winds- Zonal & Meridional	m/s
Φ	Geopotential	m
ω	Vertical Pressure Velocity	Pa/s
T	Temperature	K
θ	Equivalent Potential Temperature	K
CAPE	Convective Available Potential Energy	J/kg
CIN	Convective Inhibition	J/kg
q	Specific Humidity	g/kg
$< q >$	Total Column Water Vapor	kg/m^2
RH	Relative Humidity	
MSE	Moist Static Energy	J/kg
MSE*	Saturated Moist Static Energy	J/kg

TABLE 2.1: Used Variables

by applying cascading thresholds to separate those precipitation systems within space and to connect them in time (Skok et al., 2013). Further details about the TIMPS dataset are provided by Rajagopal et al. (2023). The domain of the TIMPS data ranges from 30.05 ºN to 30.05 ºS. However, we will only focus on systems within 25 ºN and 25 ºS to focus on MCSs that spend most of their lifetime within the tropics. The TIMPS data used covers the three-year period from 2014 to 2016 and captured around 300,000 MCSs. To conduct a climatology of MCSs throughout the tropics, a large number of these systems were required to provide precise results on their mean state while minimizing computing costs. This sample size established a baseline understanding on how tropical (no other spatial or temporal constraints) convection in MCSs evolves through time.

TIMPS was selected for this research due to its utilization of IMERG data and the FiT algorithm. Other tracking datasets use single or two-step thresholds in defining storm areas, whereas FiT's cascading thresholds are capable of detecting more nuanced MCS

features (Skok et al., 2013). Additionally, FiT allows for more object identification in its use of cascading thresholds, where they drastically redefine the system in terms of size and number of objects. As a result, more MCSs are observed and their lifetimes, even after splitting and merging events, are more accurately captured. This point, in particular, further motivated the use of TIMPS; more comprehensive MCS life cycles could be analyzed in order to analyze the links between them and precipitation and entrainment.

Since MCS sizes and lifetime limitations are crucial to the lifecycle stages' definitions, TIMPS set thresholds that precipitating systems must meet in order to be considered an MCS. First, the system must have a lifespan of at least 6 hours (Laing and Michael Fritsch, 1997, Ocasio et al., 2020). Second, the maximum precipitating area attained during the system's lifetime must reach at least 3000 km^2 (Nesbitt et al., 2000). Upper spatial bounds are not necessary, the small impact of the Coriolis force acts as a spatial limit; the average MCS length and width is significantly smaller than the Rossby radius required for a system to experience coriolis impacts (Houze Jr, 2004). Lastly, the system must contain at least one pixel at IMERG's resolution with a rain rate larger than 10 mm/hr at some point during its lifetime (Feng et al., 2021). Storms in the TIMPS data are additionally categorized by life cycle stage. Time steps with stage values of one indicate growth and initiation, two correspond to maturity, and three indicate storm decay. Life cycle stages were determined via the evolution of each storm's area and its volumetric rain rate. Together, these variables were first filtered utilizing a moving average with a window corresponding to 20% of the storm's full lifetime. The gradient of the storm's

lifetime was obtained using a centered difference. From there, maxima larger than twice of the local minima were used to mark the peak maturity of each storm. Following these maxima, each consecutive time step with areas and volumetric rain rates larger than 75% of the mature maximum were categorized as mature. Time steps before the maximum were denoted as growth steps and those after the mature period were designated as decay time steps (Rajagopal et al., 2023).

2.4 Storm-Centered Composites

A series of MCS-centered composites were collected to assess both the MCSs and their environments. The TIMPS data provides the rain-weighted center of each storm, which is used to create these storm-centered composites. This center is defined as the reference latitude and longitude (0°,0°). A 10° by 10° grid was then defined around this reference point. To exclude tropical cyclones from influencing the analysis, we exclude MCSs with grid average vorticity values larger than 10^{-4} s^{-1}. From this point, we only use the first identified instance of each storm stage per storm to avoid systems with longer time periods in certain stages influencing the composite averages. In addition to compositing horizontal grids following the storm center, vertical composites were compiled from 1000 hPa (surface) to 100 hPa (top of troposphere) at 50 hPa intervals.

2.5 Plume Buoyancy

Buoyant plumes are streams of upward movement flowing away from its source. In respect to the tropical atmosphere, this is seen in the strong convective cores that makeup and

drive MCSs. Different from the severe midlatitude storms, the upward movement of tropical MCSs cannot be treated as an isolated parcel. Instead, the convection observed in the tropics can occur with large rates of entrainment within the lower troposphere, followed by freezing condensate (Zipser, 2003). Thus, in the tropics, mixing with the environment allows for the creation of the instability required for deep convection. This mixing acts to dilute the air within the plume; suppressing low-level, weak convection and allows buoyancy to build up and break through the boundary layer towards the free troposphere (Schiro and Neelin, 2019). To analyze this, the buoyancy calculated was additionally broken down into its constituents: the influence from the undilute and dilute components. The buoyancy and its component parts are derived using the following formulae as in Adames et al. (2021):

$$e^* = 611.2e^{\frac{17.67(T-273)}{T-29.5}} \tag{2.1}$$

$$q^* = \frac{R_d}{R_v}\frac{e^*}{P*100-e^*} \tag{2.2}$$

$$MSE^* = MSE - Lq(RH-1) \tag{2.3}$$

In equation 2.2, R_v is the specific gas constant of water vapor and R_d is the specific gas constant of dry air. Plume buoyancy anomalies (B'_{tot}) were calculated using the following equations:

$$B'_u = \frac{g}{\bar{\kappa}_L \bar{T}_L c_p}(MSE'_B - MSE^{*\prime}{}_L) \tag{2.4a}$$

$$B'_d = -\frac{g w_L}{\bar{\kappa}_L \bar{T}_L c_p}(MSE'_B - MSE'_L) \tag{2.4b}$$

$$B'_{tot} = B'_d + B'_u \tag{2.5}$$

In equations 2.4a and 2.4b: g is the gravitational acceleration constant, c_P is specific heat at constant pressure, and $\bar{T}_L$ is the mean lower free tropospheric temperature. $\bar{\kappa}_L$ and w_L are unitless constants. Plume buoyancy component anomalies (B'_u and B'_d) were calculated via MSE anomalies for the boundary layer (MSE'_B), from 1000 to 850 hPa, and from MSE and MSE^* for the lower free troposphere (MSE'_L and MSE'^*_L), from 850 to 600 hPa. Starred variables indicate their saturated form and apostrophes denote anomalies. Equation 2.4a is the undilute component of the buoyancy plume while 2.4b is the dilute component.

In analysis of the thermodynamics of a convective plume, additional definitions were established to specify which parts of the composites represented the plume and the environment. With a spatial resolution of 0.5°, each composite consists of a 21 by 21 grid of individual data points. The environment was defined as the 80 points making up the four edges of the composite. This definition was set to minimize interference with the MCSs. Conversely, the plume was defined as the center data point and the 8 data points immediately surrounding it. Different definitions for both areas were analyzed, but showed no notable difference. These specifications were applied solely to the data analysis of the plume buoyancy and its dilute and undilute component parts.

Chapter 3

Analysis of Data Selection Validity

3.1 Moist Thermodynamic State

MCSs have been linked to areas of enhanced column water within the tropics, where storm initiation in particular follows the evolution of atmospheric moisture (Holloway and Neelin, 2009). In Figure 3.1, we see that TIMPS accurately captures MCS hotspots via the congruence between storm density distributions and TCW from ERA5 (Houze Jr et al., 2015). This indicates that TIMPS data spatially aligns with the ERA5 reanalysis product, the TCW, and underscores the tracking data's reliability in capturing MCSs. In Figure 3.1 we see three major regions where storm initiation density and TCW are highest. The first region is along the intertropical convergence zone (ITCZ), where TCW is above 48 kg/m^2. The ITCZ is visible in figure 3.1 from 180°W to 80°W and within a latitude band extending from the equator to 10°N. The second area of interest is the Amazon

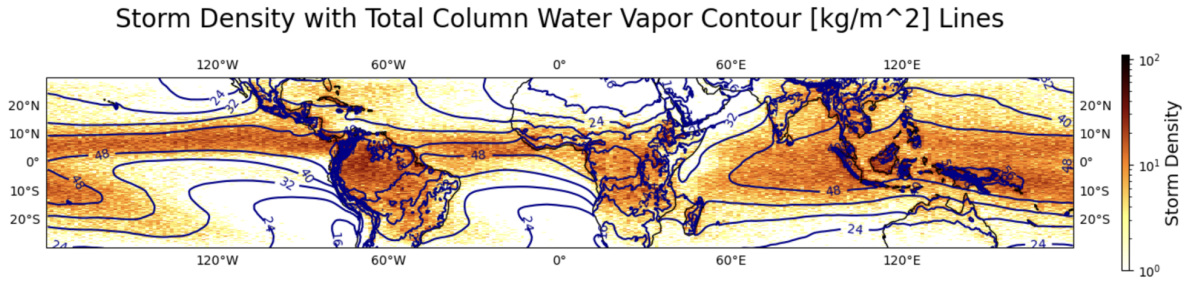

FIGURE 3.1: Density map of MCS initiations over the tropics (30°S to 30°N). Contour lines are total column water vapor [kg/m^2].

basin in northern South America, where TCW values in this region are also above 48 kg/m^2. The third region is over the Indo Pacific warm pool, which has the highest TCW values, reaching above 56 kg/m^2. Within the warm pool, there are noticeably higher concentrations of storm initiations occurring over land. This is also observed over South America and central Africa. The congruence seen here is in agreement with previous research (e.g. Houze Jr, 2004, Houze Jr et al., 2015, Pilewskie and L'Ecuyer, 2022, Schiro and Neelin, 2019, Yang and Slingo, 2001).

With increased confidence in continued use of the TIMPS tracking dataset, we now examine the distributions of column-mean ERA5 variables: CAPE, CIN, TCW, and precipitation rates during the lifetime of MCSs (Fig. 3.2). CAPE is largest in stage 1 and decreases as the life cycle progresses, while CIN is smallest in stage 1 and increases thereafter. The mode of the CAPE and CIN anomalies is roughly 25 and -10 J/kg, modest values especially considering how large CAPE and CIN fluctuations are in the midlatitudes (Johns and Doswell III, 1992). TCW anomalies display a unimodal distribution with the mode of 1 kg/m^2 at stages 1 and 2, but it develops a second mode at TCW values

of -1 kg/m^2in stage 3. Precipitation rates remain nearly uniform across different life cycle stages, with mode values close to 0 and a long tail in the distribution. There is a slightly larger range in precipitation rates during stage 2, due to the definition of life cycle stages being partly based on relative rain rates. Composite maps of CAPE, CIN, and TCW at

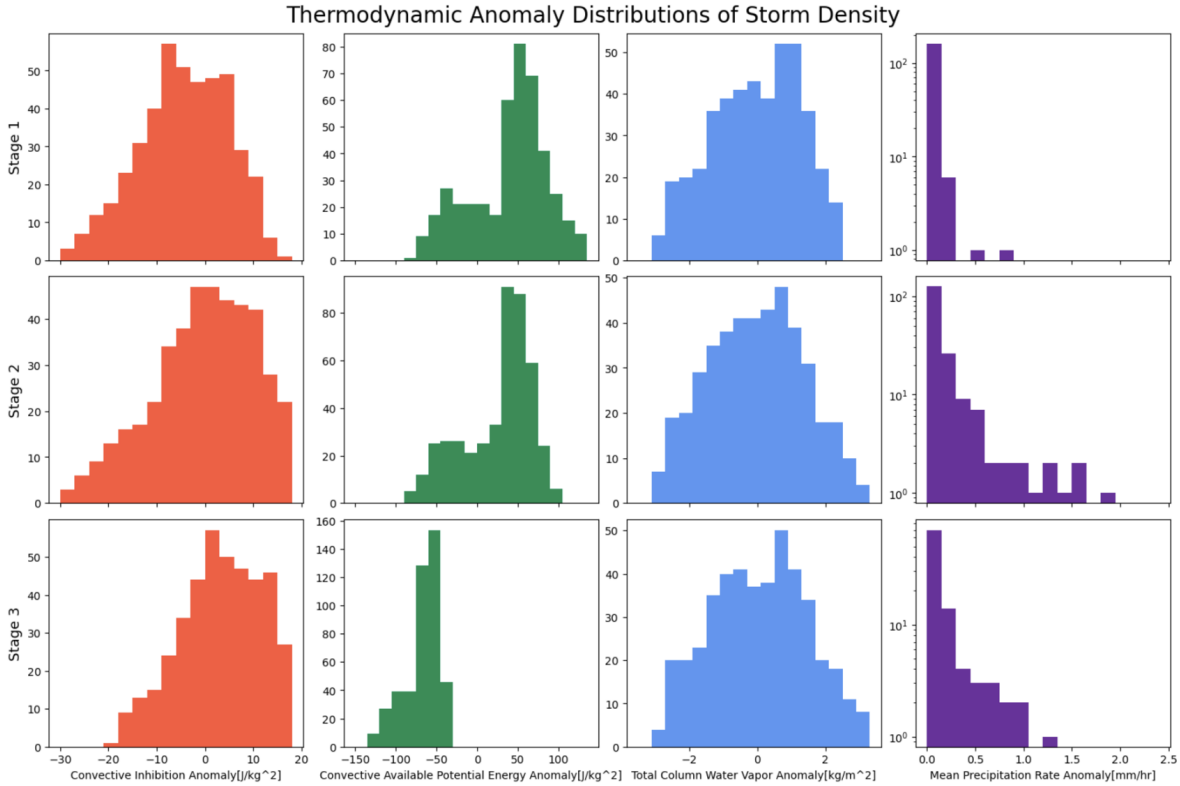

FIGURE 3.2: Barplots of CIN [J/kg^2] temporal lifetime anomalies are in orange, CAPE [kg/m^2] temporal lifetime anomalies are green, TCW [kg/m^2] temporal lifetime anomalies are blue, and spatial mean precipitation rate [mm/hr] anomalies are purple. Variable distributions are shown for each stage of the MCS life cycle.

different lifecycle stages were compiled in addition to the areal-mean temporal anomalies in Fig. 3.2 and are shown in Figure 3.3. Examining the values within a 10° by 10° grid centered on each MCS reveals discernible aerial-differences between the 3 stages. TCW shows gradual growth in the composites' centers throughout the lifetime. The largest

positive anomalies are observed in stage 3 and negative anomalies are confined to the northern and southern ends of the composites. In agreement with Fig. 3.2, we see a negative CIN anomaly greatest during stage 1 where it diminishes thereafter. In comparison to CAPE, TCW and CIN exhibit relatively small changes between the 3 stages. CAPE exhibits strong positive anomalies during stage 1 and strong negative anomalies in stage 3. Altogether, the results of this section align with what was anticipated for these bulk column-mean thermodynamics.

3.2 Precipitation in Reanalysis and Satellite Data

With the increased confidence in TIMPS' ability to capture MCSs, the next step specifically checks the accuracy of the precipitation reanalysis data. For direct comparison, we now examine the distributions of precipitation in ERA5 versus IMERG data. In Figure 3.4 we see significant disagreements between the reanalysis and satellite-based data. The IMERG data reveals substantial variations throughout the MCS life cycle, where the greatest precipitation rates are in stage 2, and the smallest are in stage 1. This is observed in the statistical distributions of precipitation rate in Fig. 3.2; stage 2 sees the largest stage-relative maximum while the smallest is observed in stage 1. ERA5's evolution and local maxima for each stage differs drastically from the IMERG observations. IMERG shows notable fluctuations in precipitation intensity across the three life cycle stages, whereas the precipitation rates for reanalysis hardly vary and grossly underestimate the maximum precipitation rate for each life cycle stage. Figure 3.5 further highlights this

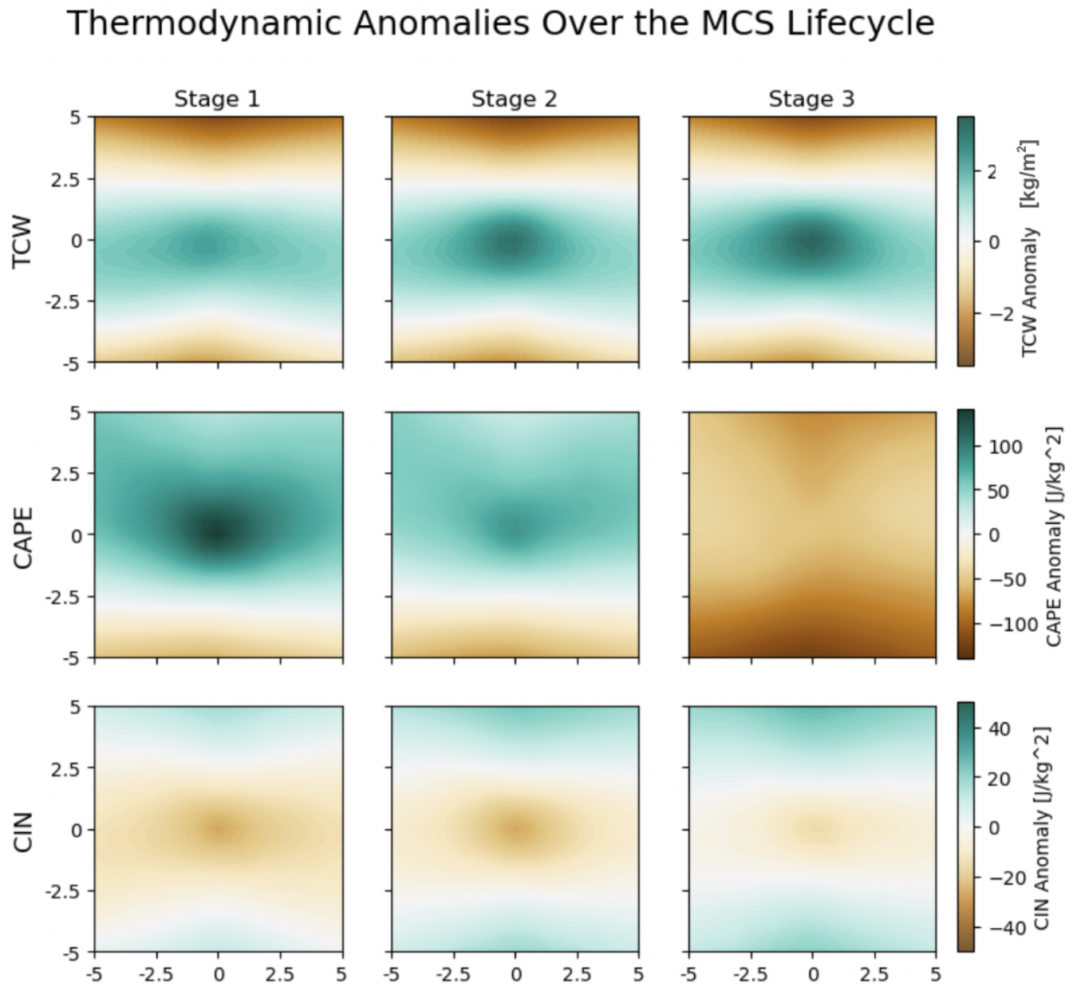

FIGURE 3.3: Areal composites of TCW [kg/m^2], CAPE [J/kg], and CIN [J/kg] temporal lifetime anomalies for each stage of the MCS life cycle.

disparity by plotting storm density as a function of each storm's corresponding ERA5 (y-axis) and IMERG (x-axis) precipitation rates. The pink line indicates a 1:1 relationship between the two datasets and is the density distribution expected if ERA5 accurately captured and modeled rain rates for each storm. The black line is the best fit line where stages 1 and 2 show a somewhat linear relationship between ERA5 and IMERG. The slopes, however, are both less than 0.2 emphasizing IMERG's larger values. The linear

relationship does not apply to the last stage, however, as the rainfall rates during stage 3 are uncorrelated.

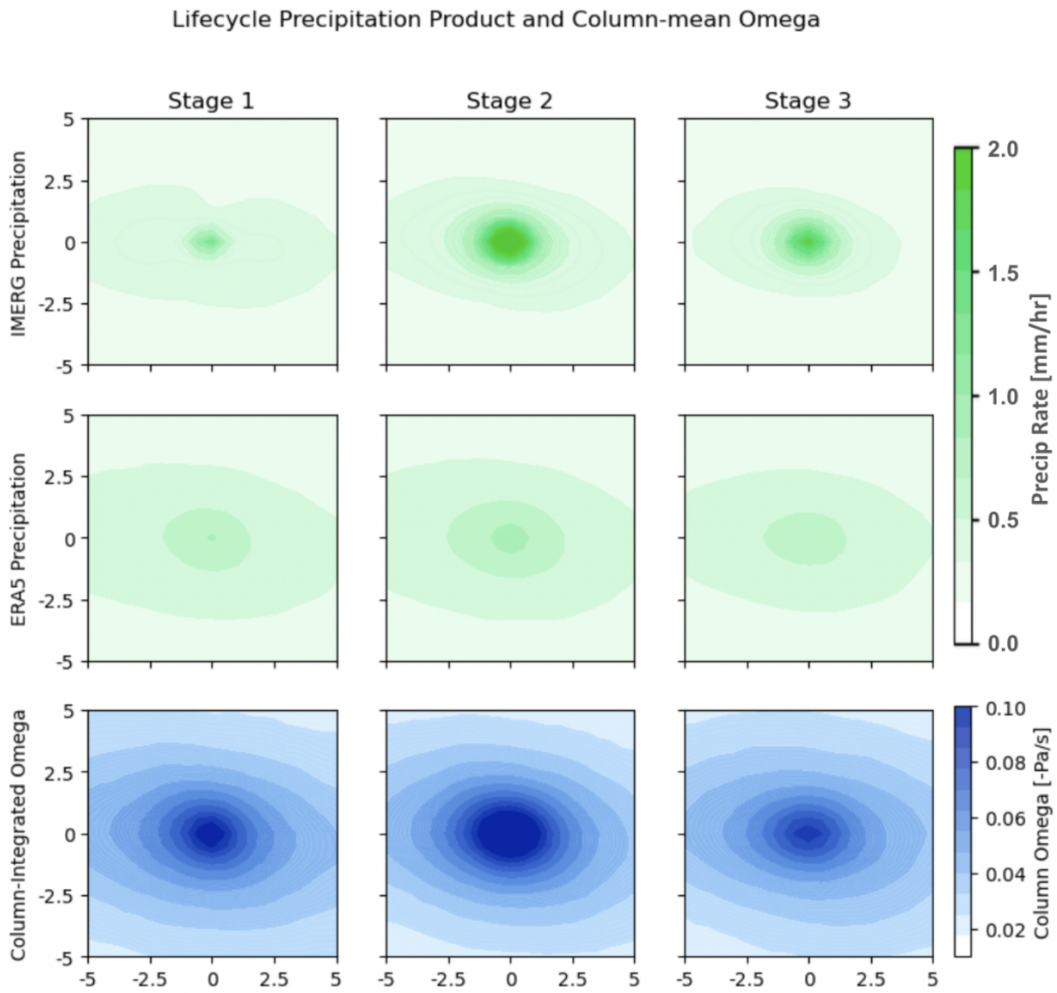

FIGURE 3.4: Areal composites of mean precipitation rate [mm/hr] from IMERG and ERA5 (top two rows) and mean column-integrated omega [-Pa/s] for each stage in the MCS lifecycle.

To further investigate the reliability of ERA5 products, we also show in Figure 3.6 the relationship between ERA5 omega and ERA5 precipitation. While the reanalysis' precipitation differed from the observations, the omega is still anticipated to increase with rising precipitation rate. In the interest of simplifying the analysis visually, omega was

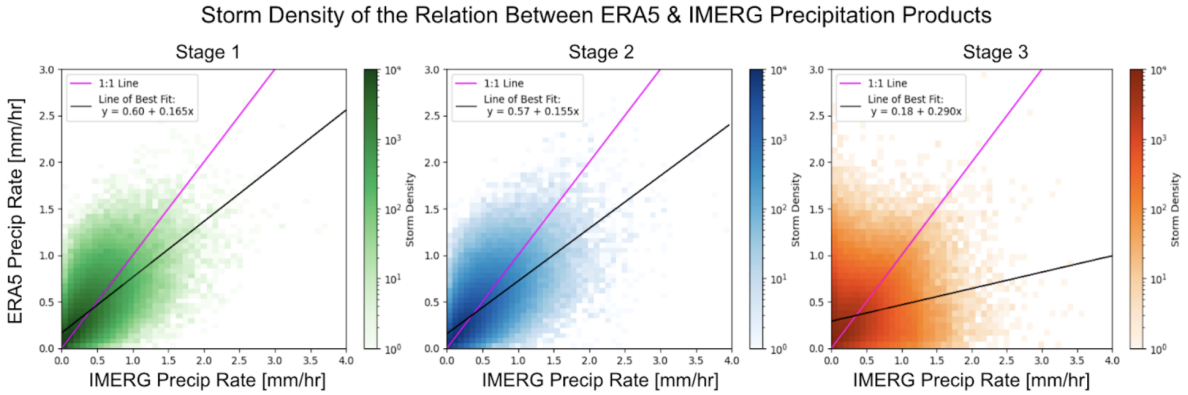

FIGURE 3.5: Storm density plots relating ERA5 and IMERG precipitation rate [mm/hr] values for each stage in the MCS life cycle: stage 1 is green, stage 2 is blue, and stage 3 is orange. Pink line indicates the 1:1 ratio while the black line is the linear line of best fit.

plotted in -Pa/s, referenced as omega continuing on, so that positive values indicate upward movement and negatives indicate downward movement. A linear correlation is observed in stages 1 and 2 of the MCS life cycle. Stage 3, however, does not appear to have a clear correlation. There is a large spread of values at this point in the life cycle, where the lifetime minimum for the correlation coefficient is observed at 0.03. In comparison to the IMERG/ERA5 precipitation products in Fig. 3.5, a similar life cycle pattern is observed: both stage 1 and 2 show loose, linear relationships while stage 3 has no discernable trends. The presence of these relationships, despite ERA5's underestimation of precipitation, strengthened our confidence in using ERA5's other environmental variables. In conjecture with Figs. 3.1 and 3.2, the confirmation of previous knowledge justifies continued use of the TIMPS and ERA5's non-precipitation variables, including temperature, specific humidity, and vertical velocity.

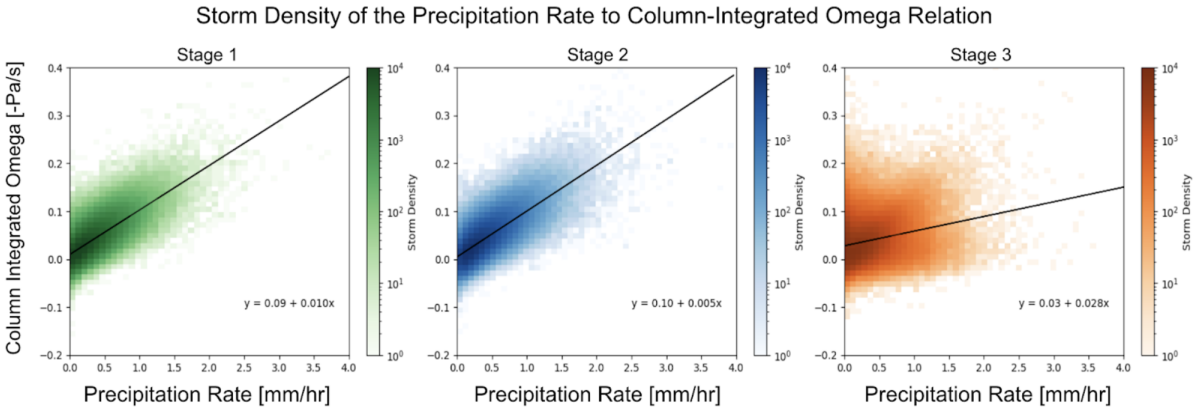

FIGURE 3.6: Storm density plots relating ERA5 precipitation rate [mm/hr] and omega [-Pa/s] values for each stage in the MCS life cycle: stage 1 is green, stage 2 is blue, and stage 3 is orange. The black line is the linear line of best fit where its equation is shown within each respective figure.

Chapter 4

Environmental Thermodynamics and Circulation Features

4.1 Vertical Motion

Before applying the plume buoyancy model, the vertical structure and movement within MCSs are needed to provide key environmental context as to what structures and relationships are present in reference to the MCS life cycle. To do so, we now look solely to the evolution of the vertical and horizontal winds throughout the MCS life cycle. These results further compound our understanding of the connections between mass and energy movement and convective precipitation rates. Figure 4.1 provides several horizontal views of the overturning circulations seen in the omega throughout the MCS life cycle at three different locations within the troposphere: 850 hPa, 500 hPa, and 200 hPa.

In stage 1, the omega reverses sign between 850 hPa and 500 hPa where upward movement lower in the atmospheric column is capped by downward flow aloft. Corroborating this, wind vector anomalies show mid-level divergence and high-level convergence. Stage 2 is dominated by upward movement throughout the entire column with the greatest anomalies in the middle free troposphere. Wind anomaly vectors, however, show little variation from the temporal, MCS-lifetime mean where deviations are very small, or nonexistent. By TIMPS' definition, the mature stage accounts for 50% of the MCS lifetime, explaining the minimal deviations from the mean state in stage 2. Even with the small variation, however, convergence is still observed at the surface with divergence at the top of the profile. Stage 3 sees an inverse relationship to stage 1, with omega reversing aloft. Small upward anomalies are observed in the 200 hPa layer with strong downward anomalies below. The wind patterns reflect this inverse pattern as well with convergence occurring in the 500 hPa layer and divergence at 200 hPa. The strongest descent is observed during this stage at the 850 hPa layer.

Figure 4.2 shows a latitude-pressure cross section of the fields shown in Fig 4.1, allowing us to examine the vertical structure of the MCS composites in more detail. There are shifts from upward motion to downward motion during stage 1, where this switch occurs near 600 hPa. The cross sectional view of stage 2 agrees with the horizontal views of Figure 4.1. Ascent is seen throughout the entire column at this stage. During stage 3, a reversal in vertical motion is observed once again, but this time it occurs at a lower pressure level near 450 hPa; this reversal aligns with expectation and is in agreement

with the results seen in Fig. 4.1.

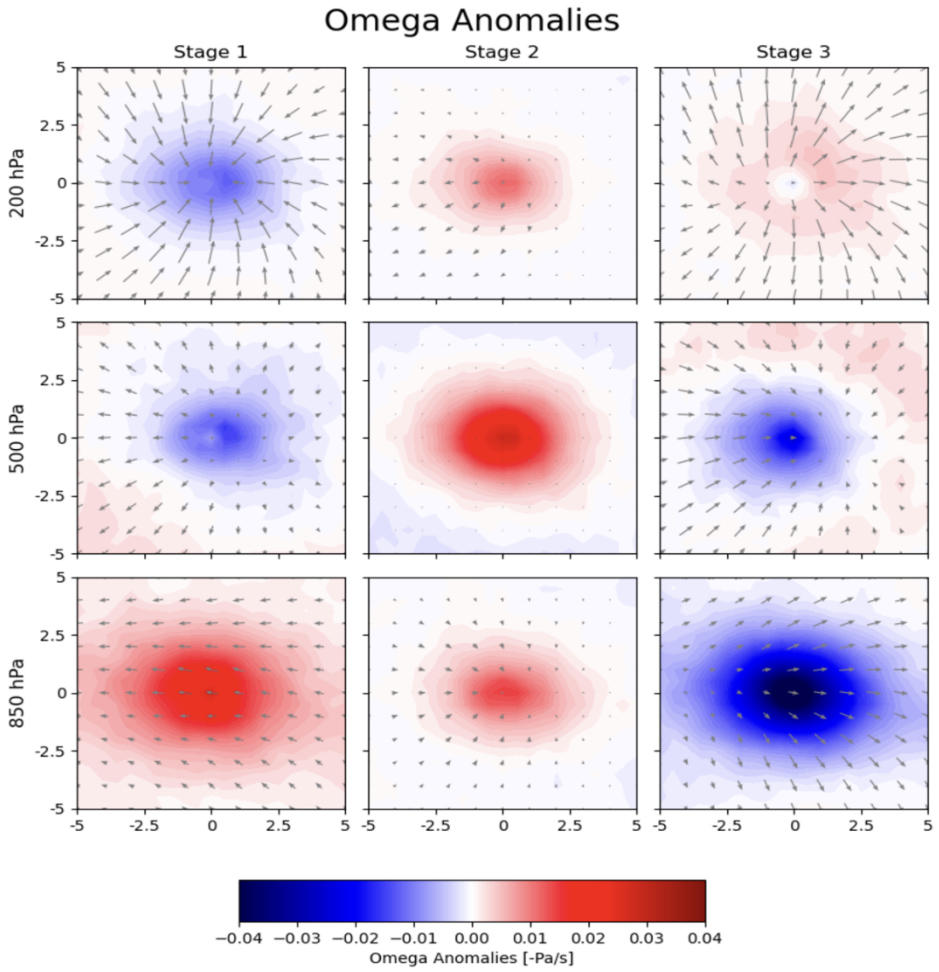

FIGURE 4.1: Areal composites of ERA5 omega temporal lifetime anomalies overlaid with arrows indicating the horizontal winds obtained from ERA5 meridional and zonal wind data for each stage in the MCS life cycle. Rows show composites at three different pressure levels: 850 hPa, 500 hPa, and 200 hPa. In the interest of simplifying the analysis visually, omega was plotted in -Pa/s, referenced as omega.

4.2 Vertical Structure Changes

With the vertical profile of how and where air is transported within MCSs established, we now explore the composited vertical structure of temperature and specific humidity

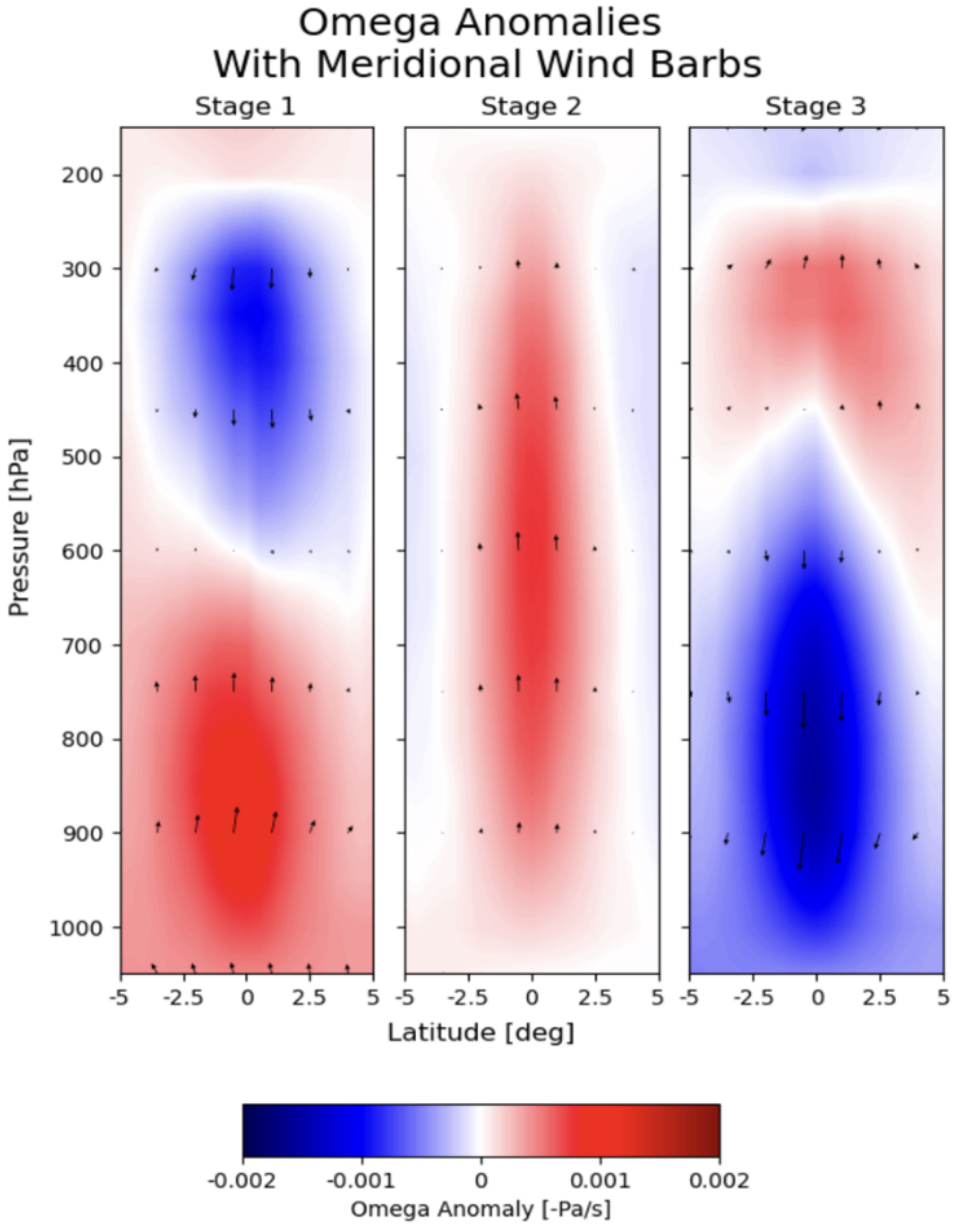

FIGURE 4.2: Latitudinally-averaged vertical profiles of minus omega [-Pa/s] from 1000 hPa to 100 hPa for each of the MCS's life cycle stages. Overlaid arrows indicate wind tendencies obtained from meridional mean winds and mean vertical velocity.

to understand mass and energy movement within them. These results aid in establishing context for the following chapter by analyzing the underlying thermodynamic-dynamic relationships present at different points in the MCS life cycle. Figure 4.3 shows vertical

composites of temperature anomalies during each of the life cycle stages. In stage 1, the greatest positive anomalies are observed at the surface and appear constrained before sharply cooling, reaching nearly 0.4 K in difference from the mean. Additionally, a smaller local maximum is present within the MFT where the temperature is around 0.1 K warmer than the lifetime mean. The low- and mid-tropospheric warmth shown in stage 1 of Fig. 4.3 is indicative of enhanced stability, which may be related to the omega profile seen in the figure's corresponding contour lines. Warm air aloft was observed to descend above this layer and may be related to enhanced clear air subsidence. Figure 4.5 shows the specific humidity anomalies in the tropospheric column for each of the stages while Figure 4.6 shows the difference anomalies from the mature stage to stage 1 and 3 as in Figure 4.4. In stage 1 of Figure 4.5, a moist anomaly is present at the surface and in the boundary layer before transitioning into a dry anomaly in the lower free troposphere near the 850 hPa pressure level. The dry anomaly peaks near 600 hPa.

When taking this pattern into consideration with the positive temperature anomalies also observed in stage 1, an interesting structure becomes evident. In convective initiation, warm and moist air at the surface is unable to rise as the dry and warm anomaly aloft prevents extensive upward acceleration. This capping-like mechanism could explain how surface and boundary layer mass and energy locally builds-up to reach the instability needed for deep convection (Wolding et al., 2016).

As observed in Figures 4.3 and 4.5, the second stage does not exhibit strong anomalies

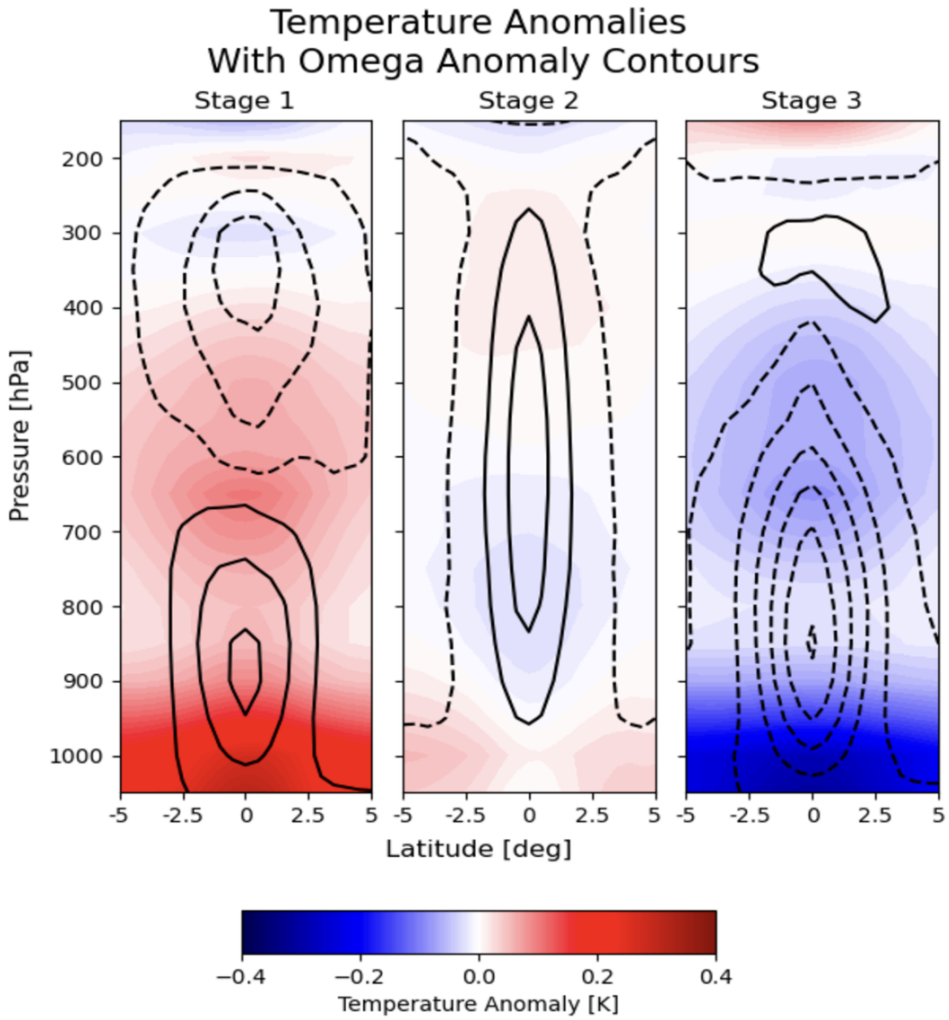

FIGURE 4.3: Longitudinally-averaged vertical profiles from 1000 hPa to 100 hPa of temporal lifetime temperature anomalies [K] for each MCS life cycle stage. Black contour lines indicate omega [-Pa/s] where solid lines represent upward movement and dotted lines represent downward movement.

in temperature and specific humidity from the lifetime's mean. Only slight deviations up to 0.05 K and 0.03 kg/m^2 are visible in the temperature and specific humidity profiles, respectively. Temperature (Figure 4.3) in the column can be seen shifting from slightly cooler to slightly warmer anomalies in the free troposphere, near 550 hPa. Specific humidity, as in Figure 4.5, shows the center of the column (from 950 to 700 hPa) dominated by

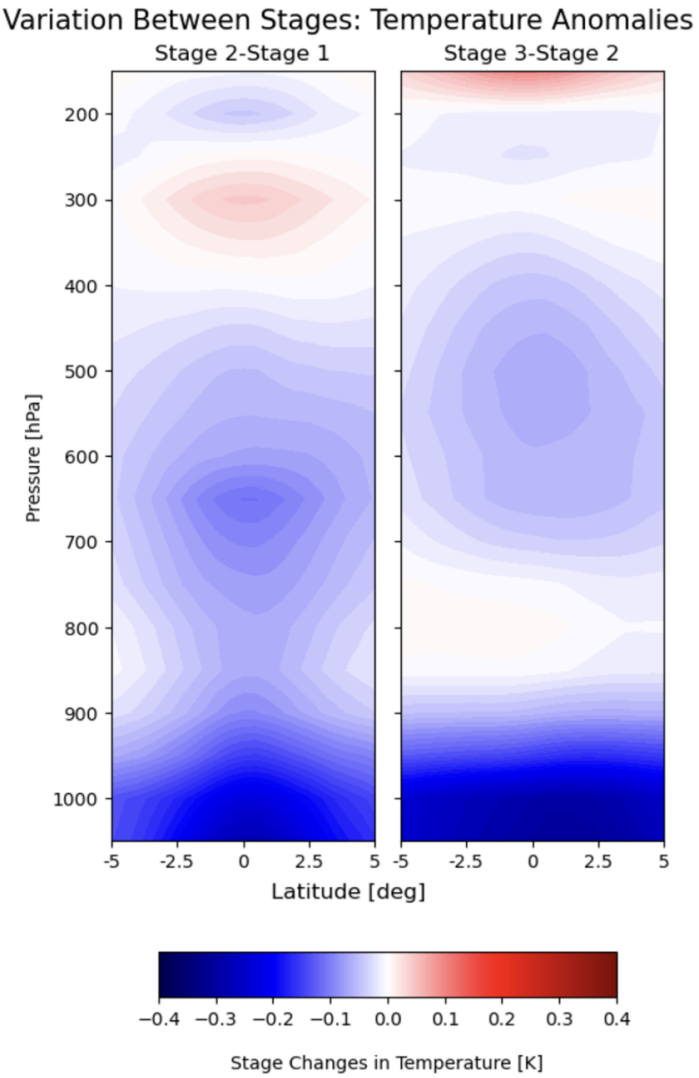

FIGURE 4.4: Longitudinally-averaged vertical profiles from 1000 hPa to 100 hPa of temporal lifetime temperature [K] anomaly differences between stage 2 and stage 1 (left panel) and stage 3 and stage 2 (right panel).

small positive anomalies that fade towards the lifetime mean as it nears the composites' edges. This enhanced moisture captures the convective cores as they mature and transport mass and energy upwards in the troposphere. At this point, the water vapor aloft condenses and precipitates out, acting to increase specific humidity in the composites' centers via moistening of the middle troposphere.

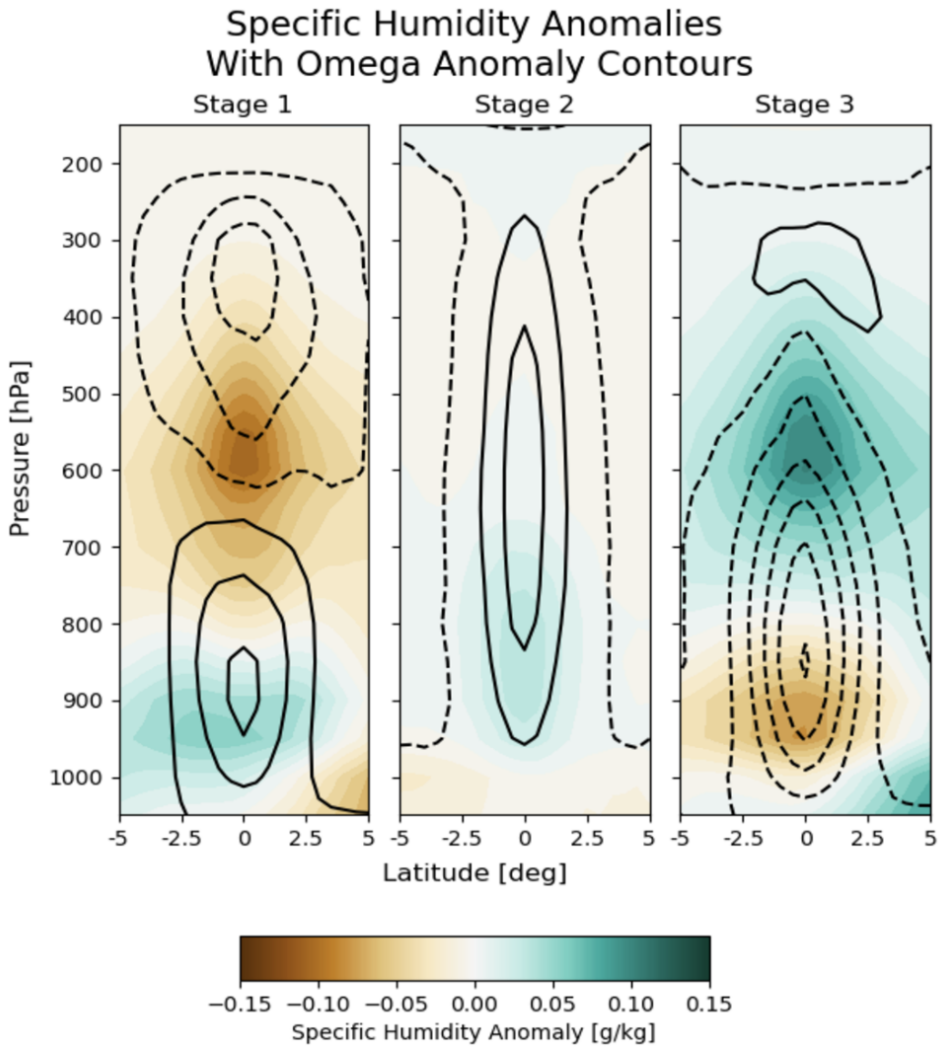

FIGURE 4.5: As in Figure 4.3 but with specific humidity [g/kg] temporal lifetime anomalies instead.

The temperature tendencies shown in stage 3 of Figure 4.3 exhibit a strong negative anomaly reaching a minimum of 0.4 K below the mean at the surface; air in this segment of the column is considerably cooler than the mean state, and may be a reflection of continuous rainfall. Additionally, the complete cessation of new and developing convection in the lower troposphere is inferred by the downward movement (as shown by negative omega anomalies) observed there. Another, albeit smaller, minimum in the temperature

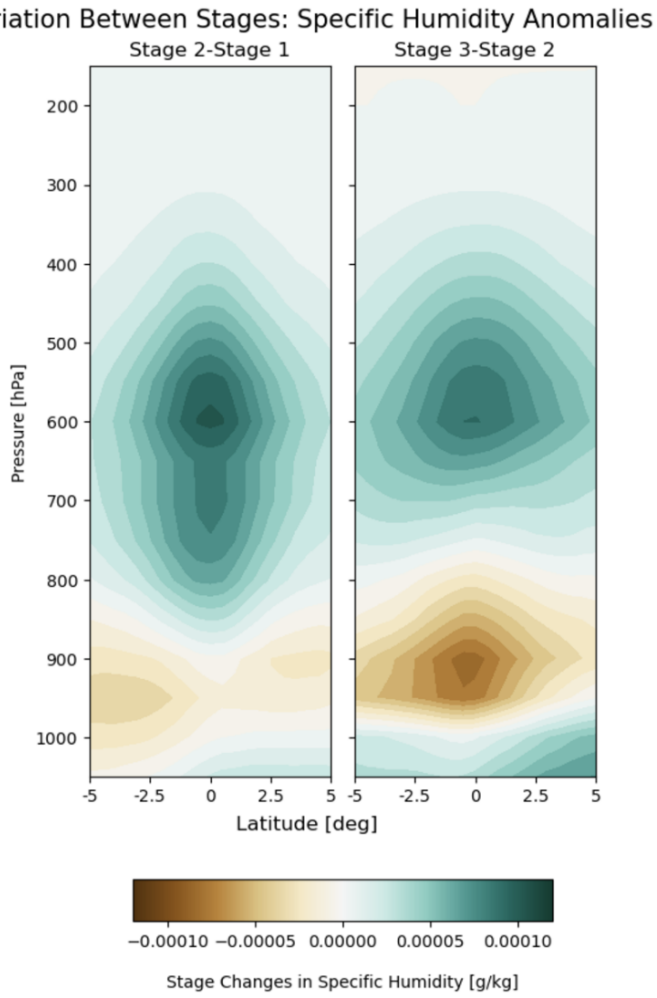

FIGURE 4.6: As in Figure 4.4 but with specific humidity [g/kg] temporal lifetime anomalies instead.

anomalies is present further aloft within the middle free troposphere near 600 hPa as per Figure 4.4. Specific humidity, however, in Figure 4.5 shows a strong dipole with anomalously moist air aloft in the lower and middle free troposphere and dry air at the boundary layer. When considering these patterns, stage 3 appears as a mirror image to stage 1. In stage 1, the column is characterized by warm and moist anomalies near the surface capped by warm and dry anomalies aloft. Stage 3, however, is an inverse reflection of this where cold and moist anomalies aloft appear to be floored by a layer of cool

and dry air in the boundary layer and at the surface. This shift from maturity, as shown in Fig 4.6, characterizes the system's transition towards a stabilizing decay state. With the vertical structures and relationships present in MCSs and their evolution through the MCS life cycle established, we can now proceed with the plume buoyancy analysis. The movement of mass and energy as discussed in this section provide the relevant context in which convective instability can be considered.

Chapter 5

Plume Buoyancy

5.1 Evolution of Plume Buoyancy in the MCS Life Cycle

We now examine the buoyancy of MCSs using the entraining plume framework as outlined in Adames et al. (2021) and described in Chapter 2: Data and Methods. Following equation 2.2, we decompose the buoyancy into its dilute and undilute components. These results, in addition to the total buoyancy (consisting both components), are shown in Figure 5.1 for each of the three MCS life cycle stages. During stage 1, we see enhanced, positive anomalies in total buoyancy near the center of the composite. These anomalies become negative as we move outward towards the composite's southern and western edges. During this stage, the undilute component contributes more to the total buoyancy

than the dilution component; the total buoyancy resembles the pattern of the undilute component. Enhanced dilution during this stage reduces the total buoyancy in the center of the MCS composite. Putting these results in reference to the life cycle omega profiles (Fig. 4.2), we see enhanced omega (upward motion) in the boundary layer and LFT corroborating the buoyancy composite; here, enhanced upward movement is indeed occurring alongside the enhanced, central core upward forcing observed within the buoyancy plots. Dry anomalies (Fig. 4.5) aloft in this stage also emphasize the stabilizing impact of dilution while the warm column anomalies (Fig. 4.3) act to strengthen the instability present in the undilute component.

The stage 2 buoyancy terms, as shown in Figure 5.1, deviate little from the spatial and temporal mean, especially in consideration of stages 1 and 3's anomalies. During this stage, the dilute and undilute components nearly cancel one another out, with the resulting total buoyancy being slightly negative. Consistent with previous research on the impacts of entrainment on a convective plume, the environment begins to grow moist which limits its drying efficiency (Inoue and Back, 2015b, Schiro and Neelin, 2019). Despite the anomalies' small magnitudes, the second stage is the point in the life cycle where the greatest upward motion and precipitation rates are observed, as seen in Figures 4.2 and 3.2. This conveys the temporal mismatch of when the greatest, positive total buoyancy anomalies versus upward motion/precipitation rate maximums are observed.

Buoyancy during Stage 3 is nearly a mirror opposite of stage 1. The buoyant state reflects the areal sign pattern of stage 2, where undilute buoyancy becomes strongly negative as

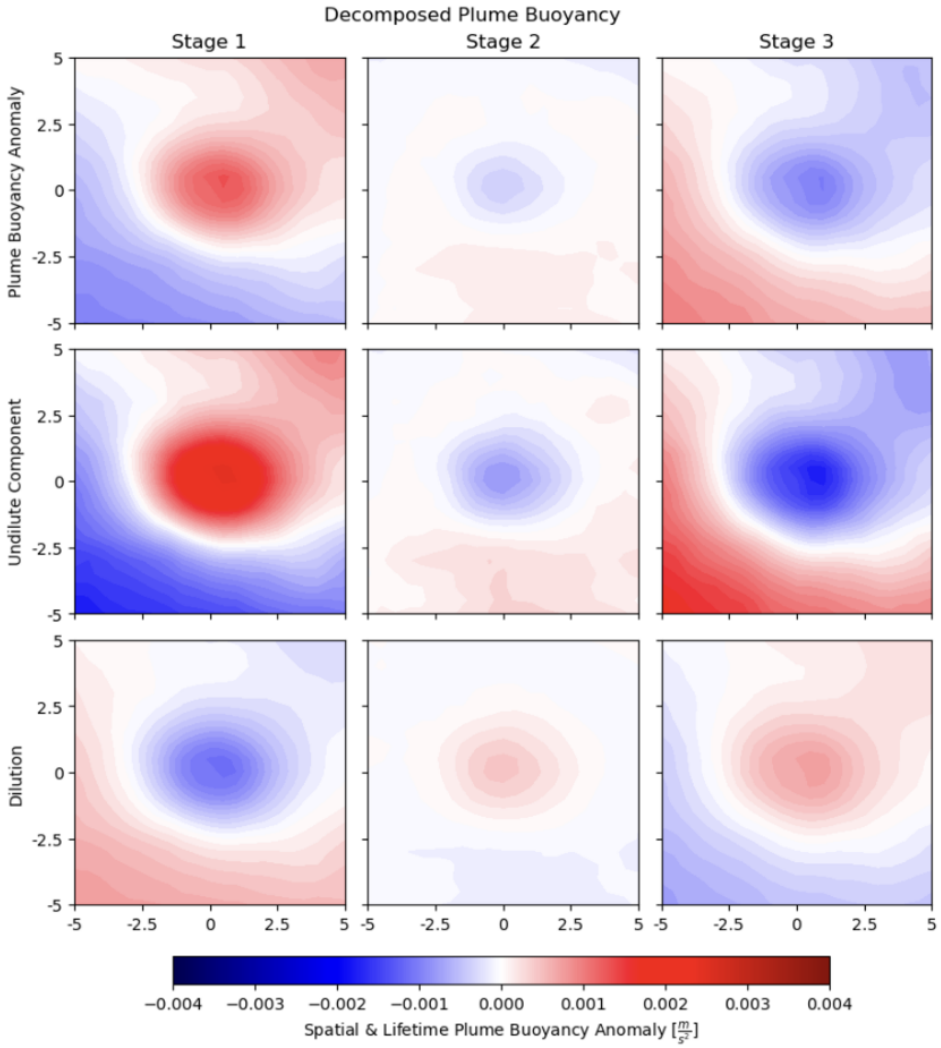

FIGURE 5.1: Decomposed plume buoyancy spatial and temporal anomalies for the three different MCS life cycle stages. Top row is total buoyancy anomaly, middle is the undilute component anomaly, and the bottom is the diluted component anomaly.

the near surface temperature anomalies become negative. In contrast, the more humid environment, as shown in Fig. 4.5, during this stage reduces the dilution of buoyancy. This is reflected in the positive dilution anomalies seen in Fig. 5.1.

The connection between the vertical motion and buoyant states of stage 3 and stage 1, as discussed previously, fits the moisture quasi-equilibrium theory on the evolution of

convection as described in Sessions et al. (2019). This is further corroborated by the low specific humidity present in the lower troposphere (Figure 4.5) and negative omega values near the surface (Figures 4.5 and 4.6). These connections are described and analyzed in Section 5: Summary and Conclusions.

5.2 Full Plume Profile of Convective Instability & Vertical Motions

To further explore the relationship between instability and vertical motion, Figure 5.2 provides a direct comparison between the grid-averaged MSE anomalies to the grid-averaged omega anomalies for the three phases of the MCS life cycle. Here, their area-mean evolution through the life cycle shows how they are interconnected through time. Stage 2, especially in its MSE anomalies, shows small deviations from the mean as these values are lifetime anomalies. The omega anomalies fit with the previous results (Fig. 4.2) where there is overall upward motion occurring through the tropospheric column. Once again, stages 1 and 3 are near mirror images of one another; these values were obtained via ERA5 and were not calculated from a lifetime or spatial average. These results are pure reflections of the vertical profiles' anomalous states; this is important to note as the connections between MSE and omega are clear in both their relationship to one another and their evolutions through the life cycle.

Omega anomalies in stage 1 are positive at the surface, indicating enhanced buoyancy, and negative aloft, indicating suppressed buoyancy. Additionally, the lifetime omega

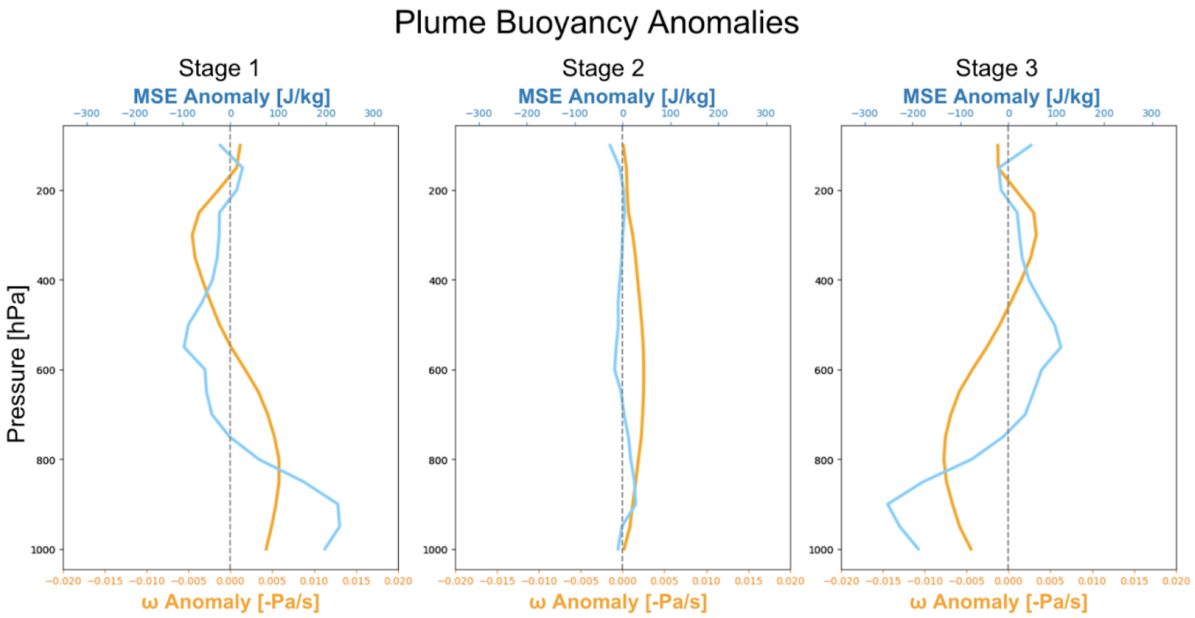

FIGURE 5.2: Vertical profiles from 1000 hPa to 100 hPa of moist static energy [J/kg]temporal lifetime anomalies in blue and omega anomalies [-Pa/s] in orange for each MCS life cycle stage.

maximum (strongest updrafts) is observed near the surface in stage 1 (Fig. 5.2). These results are consistent with current diagnostic theory on the structures of MSE and omega within both convectively enhanced and suppressed periods (Benedict et al., 2014, Hannah and Maloney, 2011, 2014, Inoue and Back, 2015b, Masunaga and L'Ecuyer, 2014, Sobel et al., 2014). This interaction between MSE and omega is referenced as gross moist stability (GMS) within said research (Neelin and Held, 1987). Stage 1 is characterized by negative GMS where it is associated with enhancing convection; this is shown in Fig. 5.2 where the tropospheric profile shows enhanced MSE in the lower portions and diminished MSE in the middle of the profile. This is the result of the eventual net import of MSE from surrounding vertical circulation which acts to destabilize and moisten the tropospheric column.

Stage 3 sees the reverse of the structure present in stage 1: omega anomalies are negative in the lower portion of the tropospheric column and positive aloft in the middle free troposphere. Also, the lifetime minimum of omega is present at the surface in stage 3. Thus, as a reflection of stage 1, stage 3 likely exhibits positive GMS with higher MSE aloft in the upper troposphere and lower amounts in the middle free troposphere; the structures seen in Figure 5.2 support this. The associated vertical motions lead to the export of moisture via MSE, leading to stabilization and drying of the column and eventual convective decay (Inoue and Back, 2015b). Through this analysis, the importance of atmospheric moisture's concentration, movement, and location within the troposphere is emphasized. And while consistent with previous research on GMS and the impacts of environmental mixing on buoyancy/convection, the lifetime omega maximum present at the bottom of the tropospheric column and the net positive plume buoyancy (Figure 5.1) in stage 1 suggest contention with moisture quasi-equilibrium.

Chapter 6

Summary & Conclusions

6.1 Addressing the Hypotheses

Looking to better understand the thermodynamics that drive mesoscale-convection, this study utilized a novel MCS storm tracking dataset to address the main question: How do buoyancy and moisture affect isolated tropical MCSs throughout their life cycles? In response to this question, we posited two hypotheses to understand the role of buoyancy and moisture in the MCS life cycle; to test these hypotheses, we carried out a composite analysis following the three stages of the MCS life cycle, as shown in Figure 1.2, using the TIMPS data set and ERA5/IMERG data. Results from this analysis provide the following answers to our hypotheses.

Hypothesis 1: Enhanced moisture in the lower troposphere evolves with convection, where maximum column moisture occurs alongside maximum updraft speeds, buoyancy, and precipitation.

First focusing on observations of MCS initiation, we saw warm, dry air aloft acting to cap and prevent further vertical development. In stabilizing the atmosphere at this level, boundary layer and LFT mass and energy locally accumulates. This restriction in vertical motion is confirmed by the composited vertical omega profiles (Figures 4.2 and 4.3) where negative anomalies halt near 700 hPa, within the free troposphere, and where clouds remain shallow. Figure 6.1 illustrates those present patterns in the specific humidity, vertical motions, and cloud morphology. The relation between these variables by extension then act as key components in the ability of convective plumes to continue building, and eventually precipitating out. The highest values of instability (buoyancy) are anticipated to coexist with the highest rates of precipitation within an MCS's life. We show that large accumulations of surface moisture and boundary layer and LFT instability are linked to the vertical development that large-scale precipitation requires. This highlights the crucial importance of having enough lower-tropospheric moisture build in order for deep convection to occur in the first place. The observed dry and warm cap at 700 hPa is thus a necessary structure for the build-up of the local moisture and buoyancy building tropical convective systems require.

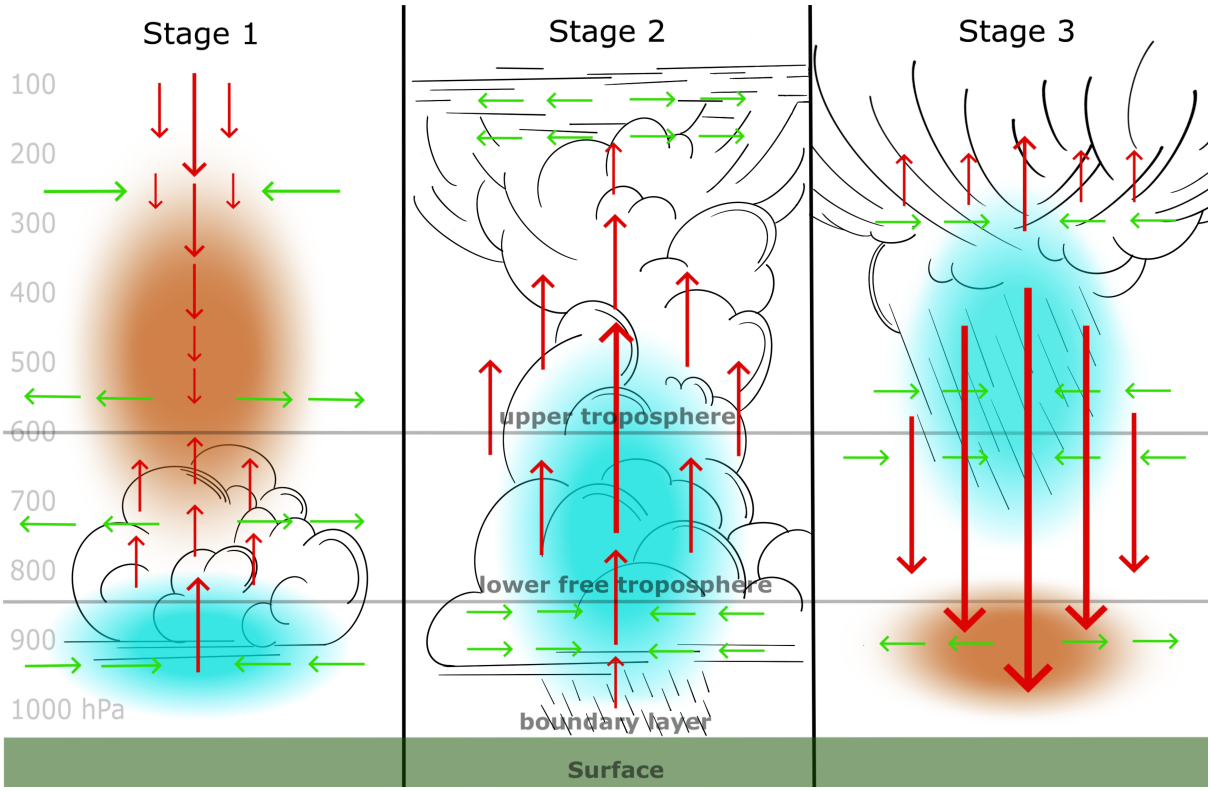

FIGURE 6.1: Schematic of anticipated cloud structures based on obtained results. Blue indicates areas of enhanced specific humidity and vice versa for tan areas and is based on the results shown in Fig. 4.5. Green arrows indicate horizontal winds, as shown in Fig. 4.1, and the subsequent areas of convergence/entrainment and divergence/detrainment. Red arrows indicate vertical motions, as shown in Fig. 4.2. Profiles are separated into four areas: the surface, boundary layer (1000-850 hPa), lower free troposphere (850-600 hPa), and the upper troposphere (600-100 hPa).

Shifting to focus on the temporal evolution of lower-tropospheric moisture, it arises as an important element in the development and initiation of tropical deep convection. However, discrepancies with previous research were observed between the moisture-buoyancy relationship when the entire MCS life cycle is considered in the analysis (Inoue and Back, 2015a, Schiro et al., 2018, Schiro and Neelin, 2019). Looking specifically at precipitation rate trends, there is a notable pattern present which deviates from moisture quasi-equilibrium. Figure 6.1 shows positive plume buoyancy anomalies occurring in

stage 1 while Figure 4.4 shows the greatest precipitation rates occurring within stage 2. Under moisture quasi-equilibrium, a buoyant plume is anticipated to entrain dry air thus decreasing the buoyancy; this causes upward motions to halt, evaporation to disperse remaining moisture, and detrainment of the vapor into the surrounding atmosphere. Under this framework, convection relies on the continuous creation of new convective plumes in order to establish a moist environment where latent heating (via condensation in moist, rising plumes) stabilizes and deepens the convective core plume (Sessions et al., 2019).

This suggestion that moist convection uses potential energy at the rate in which it is provided via larger scale processes is not seen in the results of this research when the entire MCS life cycle is considered; instead, a temporal gap is present between greatest plume buoyancy (Fig. 5.1) and moisture/precipitation (Figs. 3.3 and 4.5) in terms of which life cycle stage they occur. The existence of a warm and dry capping layer (Fig. 4.3) does act to follow moisture quasi-equilibrium when only convective initiation is considered. However, when analyzed with the observation that greatest lifetime plume buoyancy occurs during stage 1, they together diverge from moisture quasi-equilibrium. Under said framework, the most stable environments should additionally be the moistest; the MCS life cycle breaks from this in the time lapse observed between greatest plume buoyancy (i.e. stage 1), precipitation rates (i.e. stage 2), and moisture (i.e. stage 3) (Sessions et al., 2019). Stage 3 has the highest humidity and stability, but the total plume buoyancy observed is still negative. Moisture quasi-equilibrium does not account for external dynamics, such as the influence of gravity waves and their dissipation, and may explain the disconnect observed in our results (Adames Corraliza et al., 2024). An

interesting development, this result directly disagrees with our hypothesis that maximum updraft speeds, buoyancy, and precipitation coevolve throughout the MCS life cycle.

Hypothesis 2: Updraft dilution by mixing with the environment acts to suppress buoyancy and is the leading contributor to MCS decay.

The different vertical profiles MCSs see throughout their life were covered in this research. In reference to modern theories on the mechanics and structures that make up tropical deep convection, we address the second hypothesis and look at the relevance mixing and dilution play in the evolution of a convective plume. Contemporary research has emphasized how MCS structure continues to evolve with the entrainment of high potential vorticity and buoyancy (Schiro and Neelin, 2019). As shown previously, horizontal (meridional and zonal) winds within the vertical structure of the troposphere consist of convergence at the bottom of the active convective cell and divergence aloft. These structures result in environmental air being brought into the bottom of the plume acting to mix before it is carried aloft through the column. Arising as a result of buoyant motions, surface level convergence, which acts to bring in environmental air, was present in both stages 1 and 2. During MCS decay, the convergent wind pattern occurred at a higher elevation; here, moistened air from the middle free troposphere is brought into the plume and mixes. As new convection creation ceases, the upper troposphere is left as a moist and cool region.

Having established the occurrence of mixing at multiple pressure levels for each stage in the MCS life cycle, further conclusions can be inferred. In context with mixing, a relationship arises between precipitation, buoyancy, and vertical motion (omega). As shown in section 3, stages 1 and 2 saw positive, linear relationships between omega and precipitation rates. When considering how vertical motions arise as an expression of mass conservation by causing convergence at lower levels and divergence aloft, omega becomes a useful metric in indicating how mixing exerts impacts on MCS structures and their evolutions. Focusing on stage 1, upward vertical motions were confined to the lower troposphere where, as shown in Fig 5.1, undilute (unmixed) air exerts more influence on the buoyancy as opposed to the dilute component. Stage 2 observed near-mean total buoyancy arising as the dilute and undilute components act to cancel one another out; here, the convective plume was observed throughout the entirety of the profile. Stage 3, however, diverges from our hypothesis where the undilute component is the dominant influence. Figure 5.2 showed low MSE values near the surface and positive vertical motions in the upper free troposphere (Figure 4.2) occurring in MCS decay. This indicates the moisture present in the upper troposphere is acting to stabilize the environment and directly disagrees with our hypothesis. With impacts from the dilute component suppressed, the dilute and undilute components do not cancel one another out as moisture quasi-equilibrium stipulates. As a result, enhanced undilute component is associated with the stabilization of the lower troposphere and the inevitable cessation of convective plume creation and disagrees with our hypothesis.

6.2 Stipulations in Using ERA5 Data

A significant caveat that must be kept in mind in the reading of the results arises in terms of reanalysis data's accuracy and reliability. The reanalysis used here was from ERA5; not an observation product, this data instead provides the best estimate of the real state of the atmosphere. Models are used to fill in the blanks left behind by observations in order to produce temporally and spatially higher-resolved products. Many of the variables used in this research, including MSE and vertical velocity, rely on model outputs as they have components unable to be either measured remotely or at the resolution needed (Wolding et al., 2022).

Figures 3.3 and 3.4 reflect some of the issues associated with using reanalysis data. In analysis of the precipitation data specifically, ERA5, a reanalysis product, was compared to observations via IMERG data. Significant disagreements were found between the two in terms of overall lifetime precipitation rate averages as well as the course and magnitude of said rate's evolution through time and space. An example of these disagreements lies in analysis on the decay stage of the MCS life cycle where no discernable patterns were observed between ERA5 and IMERG data. Reasons for such discrepancies are yet to be fully understood, but a large portion of the variance may be attributed to the on-going investigation of stratiform growth and structures in MCSs. At the moment of this writing, capturing and modeling significant changes in the stratiform deck of mature and decaying MCSs remains difficult. Such disagreements, especially in the tropics, are a well-known downside of utilizing reanalysis (Xin et al., 2021). The processes behind

precipitation formation in tropical mesoscale storms remain an area of active research and thus partially drive our own future research endeavors in determining the physical mechanisms underlying tropical convection.

Another issue that arose in the course of this research pertains to the disagreements between the omega and precipitation values analyzed; figs. 3.4 and 3.6 highlight this disparity. One possible explanation lies in the algorithms of the storm tracking dataset used to create our areal composites of MCS life cycle stages. In it, the definition of the spatial bounds used are well-known to experience difficulties in accurately following consecutive objects through different time steps. Fast-propagating MCSs within a sheared environment and long time gaps between consecutive time steps are both capable of moving and shifting a system faster than what can be captured in certain temporal resolutions. Beyond the tracking algorithm, however, the likely culprit for the omega-precipitation disagreements lies in the reanalysis's precipitation product. Previous research has shown there are biases in certain ERA5 products. Precipitation rates and accumulations are consistently underestimated; ERA5 struggles to accurately model highest-observed precipitation values (Lavers et al., 2022). General locations and large-scale patterns are still captured, but do not apply within the scope of this research. As such, the results of this research must be interpreted with these limitations in mind; addressing these limitations is included in our anticipated future analysis.

The tropics, in particular, stand out as an area where ERA5 struggles to accurately capture the mechanisms present. Vitart et al. (2022) showed ERA5 struggled with forecasting

convective precipitation, even when utilizing a 12 hour lead. Reasons for this disparity were shown to be a result of the ERA5 model misrepresenting upper-level divergence. Potential further error may lie in the disparities present within the interactions between convection and surface anomalies (Lavers et al., 2022). While these disagreements may be a caveat to our research, they help to identify ways in which reanalysis can be adjusted to more accurately describe the state of the atmosphere.

6.3 Future Plans and Applications

With the current composite data, future endeavors will include significance and impact studies of storm location; continental and oceanic systems will be compared and further regional dependence will be explored. Current research has begun to address these regional differences (Galarneau Jr et al., 2023, Houze Jr, 2004, 2014, Schumacher and Rasmussen, 2020). Additionally, as shown in Fig. 3.1, concentrations of MCS occurrence varies widely across the tropics where different environmental factors may influence convection in different ways. To address ERA5's underestimation of precipitation rates, it will be calculated as a residual from the dry static energy budget. Constrained by observations, this method may produce better precipitation estimates from the reanalysis used (Back and Bretherton, 2009). Profile analysis of the buoyancy and its component terms will additionally be considered; uncertainty still lies in the vertical distribution and impact of buoyant forces above the boundary layer and LFT. Further analysis will include cloud morphology data from CloudSat (Stephens et al., 2008) and CALIPSO (Winker et al., 2010) satellites with the goal to better understand the disagreements between IMERG

and ERA5 during MCS decay. Exploring alternate definitions of the decay stage, such as the charging and discharging cycles highlighted in Wolding et al. (2020), could also help us better understand this discrepancy.

6.4 An Afterword

Lastly, the research and hypotheses surrounding this topic must be considered within the mindframe of real world impacts and implications. Despite ongoing progress in the research and understanding of tropical deep convection, the humanitarian motivation still remains. The tropics contain 40% of the human population (Edelman et al., 2014). The processes that occur within the tropics are thus vital to the livelihood of these people, and are also fundamental to the stability of earth's climate in the redistribution of global energy Zipser (2003). MCSs are notorious for producing dangerous conditions including strong winds, landslides, and lightning, any of which are capable of significant damage and may lead to loss of life (Engel et al., 2017, Rajagopal et al., 2023). Better understanding of the relationship between tropical deep convection and MCS structures and evolutions ultimately mean better simulation of them in both climate and forecasting models, acting to save lives by improving severe tropical storm forecasting and preparedness.

Bibliography

Adames, A. F., 2022: The basic equations under weak temperature gradient balance: Formulation, scaling, and types of convectively coupled motions. *Journal of the Atmospheric Sciences*, **79**, 2087 – 2108, doi:10.1175/JAS-D-21-0215.1.

Adames, A. F., S. W. Powell, F. Ahmed, V. C. Mayta, and J. D. Neelin, 2021: Tropical precipitation evolution in a buoyancy-budget framework. *Journal of the Atmospheric Sciences*, **78**, 509 – 528, doi:10.1175/JAS-D-20-0074.1.

Adames Corraliza, A. F., V. C. Mayta, F. Ahmed, B. O. Wolding, and K. A. Schiro, 2024: Damped gravity waves, weak temperature gradients, and tropical deep convection, submitted.

Ahmed, F., Á. F. Adames, and J. D. Neelin, 2020: Deep convective adjustment of temperature and moisture. *Journal of the Atmospheric Sciences*, **77**, 2163–2186.

Ahmed, F. and J. D. Neelin, 2018: Reverse engineering the tropical precipitation–buoyancy relationship. *Journal of the Atmospheric Sciences*, **75**, 1587–1608.

Ahmed, F. and C. Schumacher, 2015: Convective and stratiform components of the precipitation-moisture relationship. *Geophysical Research Letters*, **42**, 10–453.

Arakawa, A. and W. H. Schubert, 1974: Interaction of a cumulus cloud ensemble with the large-scale environment, part i. *Journal of the atmospheric sciences*, **31**, 674–701.

Back, L. E. and C. S. Bretherton, 2009: A simple model of climatological rainfall and vertical motion patterns over the tropical oceans. *Journal of Climate*, **22**, 6477–6497.

Benedict, J. J., E. D. Maloney, A. H. Sobel, and D. M. Frierson, 2014: Gross moist stability and mjo simulation skill in three full-physics gcms. *Journal of the Atmospheric Sciences*, **71**, 3327–3349.

Berg, L. K. and R. B. Stull, 2002: Accuracy of point and line measures of boundary layer cloud amount. *Journal of Applied Meteorology and Climatology*, **41**, 640–650.

Edelman, A., A. Gelding, E. Konovalov, R. McComiskie, A. Penny, N. Roberts, S. Templeman, D. Trewin, M. Ziembicki, B. Trewin, et al., 2014: State of the tropics 2014 report.

Engel, T., A. H. Fink, P. Knippertz, G. Pante, and J. Bliefernicht, 2017: Extreme precipitation in the west african cities of dakar and ouagadougou: Atmospheric dynamics and implications for flood risk assessments. *Journal of Hydrometeorology*, **18**, 2937–2957.

Feng, Z., L. R. Leung, N. Liu, J. Wang, R. A. Houze Jr, J. Li, J. C. Hardin, D. Chen, and J. Guo, 2021: A global high-resolution mesoscale convective system database using

satellite-derived cloud tops, surface precipitation, and tracking. *Journal of Geophysical Research: Atmospheres*, **126**, e2020JD034202.

Galarneau Jr, T. J., X. Zeng, R. D. Dixon, A. Ouyed, H. Su, and W. Cui, 2023: Tropical mesoscale convective system formation environments. *Atmospheric Science Letters*, **24**, e1152.

Hannah, W. M. and E. D. Maloney, 2011: The role of moisture–convection feedbacks in simulating the madden–julian oscillation. *Journal of Climate*, **24**, 2754–2770.

— 2014: The moist static energy budget in ncar cam5 hindcasts during dynamo. *Journal of Advances in Modeling Earth Systems*, **6**, 420–440.

Hayden, L., C. Liu, and N. Liu, 2021: Properties of mesoscale convective systems throughout their lifetimes using imerg, gpm, wwlln, and a simplified tracking algorithm. *Journal of Geophysical Research: Atmospheres*, **126**, e2021JD035264.

Holloway, C. E. and J. D. Neelin, 2009: Moisture vertical structure, column water vapor, and tropical deep convection. *Journal of the atmospheric sciences*, **66**, 1665–1683.

Houze Jr, R. A., 2004: Mesoscale convective systems. *Reviews of Geophysics*, **42**.

— 2014: *Cloud dynamics*. Academic press.

Houze Jr, R. A., K. L. Rasmussen, M. D. Zuluaga, and S. R. Brodzik, 2015: The variable nature of convection in the tropics and subtropics: A legacy of 16 years of the tropical rainfall measuring mission satellite. *Reviews of Geophysics*, **53**, 994–1021.

Huffman, G. J., D. T. Bolvin, D. Braithwaite, K.-L. Hsu, R. J. Joyce, C. Kidd, E. J. Nelkin, S. Sorooshian, E. F. Stocker, J. Tan, et al., 2020: Integrated multi-satellite retrievals for the global precipitation measurement (gpm) mission (imerg). *Satellite precipitation measurement: Volume 1*, 343–353.

Huffman, G. J., D. T. Bolvin, E. J. Nelkin, E. F. Stocker, and J. Tan, 2019: V06 imerg release notes. *NASA/GSFC: Greenbelt, MD, USA*, **355**.

Inoue, K. and L. Back, 2015a: Column-integrated moist static energy budget analysis on various time scales during toga coare. *Journal of the Atmospheric Sciences*, **72**, 1856–1871.

Inoue, K. and L. E. Back, 2015b: Gross moist stability assessment during toga coare: Various interpretations of gross moist stability. *Journal of the Atmospheric Sciences*, **72**, 4148–4166.

Johns, R. H. and C. A. Doswell III, 1992: Severe local storms forecasting. *Weather and Forecasting*, **7**, 588–612.

Kingsmill, D. E. and R. A. Houze Jr, 1999: Thermodynamic characteristics of air flowing into and out of precipitating convection over the west pacific warm pool. *Quarterly Journal of the Royal Meteorological Society*, **125**, 1209–1229.

Laing, A. G. and J. Michael Fritsch, 1997: The global population of mesoscale convective complexes. *Quarterly Journal of the Royal Meteorological Society*, **123**, 389–405.

Lavers, D. A., A. Simmons, F. Vamborg, and M. J. Rodwell, 2022: An evaluation of era5 precipitation for climate monitoring. *Quarterly Journal of the Royal Meteorological Society*, **148**, 3152–3165.

Liu, C. and M. W. Moncrieff, 2007: Sensitivity of cloud-resolving simulations of warm-season convection to cloud microphysics parameterizations. *Monthly weather review*, **135**, 2854–2868.

Liu, N., L. R. Leung, and Z. Feng, 2021: Global mesoscale convective system latent heating characteristics from gpm retrievals and an mcs tracking dataset. *Journal of Climate*, **34**, 8599–8613.

Masunaga, H. and T. S. L'Ecuyer, 2014: A mechanism of tropical convection inferred from observed variability in the moist static energy budget. *Journal of the Atmospheric Sciences*, **71**, 3747–3766.

Moncrieff, M. W. and M. J. Miller, 1976: The dynamics and simulation of tropical cumulonimbus and squall lines. *Quarterly Journal of the Royal Meteorological Society*, **102**, 373–394.

Neelin, J. D. and I. M. Held, 1987: Modeling tropical convergence based on the moist static energy budget. *Monthly Weather Review*, **115**, 3–12.

Nesbitt, S. W., E. J. Zipser, and D. J. Cecil, 2000: A census of precipitation features in the tropics using trmm: Radar, ice scattering, and lightning observations. *Journal of climate*, **13**, 4087–4106.

Ocasio, K. M. N., J. L. Evans, and G. S. Young, 2020: A wave-relative framework analysis of aew–mcs interactions leading to tropical cyclogenesis. *Monthly Weather Review*, **148**, 4657–4671.

Pilewskie, J. and T. L'Ecuyer, 2022: The global nature of early-afternoon and late-night convection through the eyes of the a-train. *Journal of Geophysical Research: Atmospheres*, **127**, e2022JD036438.

Rajagopal, M., J. Russell, G. Skok, and E. Zipser, 2023: Tracking mesoscale convective systems in imerg and regional variability of their properties in the tropics. *Journal of Geophysical Research: Atmospheres*, **128**, e2023JD038563.

Raymond, D., Ž. Fuchs, S. Gjorgjievska, and S. Sessions, 2015: Balanced dynamics and convection in the tropical troposphere. *Journal of Advances in Modeling Earth Systems*, **7**, 1093–1116.

Riehl, H. and J. Malkus, 1958: On the heat balance in the equatorial trough zone. *Geophysica*, **65**, 1–14.

Roca, R. and T. Fiolleau, 2020: Extreme precipitation in the tropics is closely associated with long-lived convective systems. *Communications Earth & Environment*, **1**, 18.

Russell, J., 2021: Timps dataset. Accessed on May, 2023, dataset.

URL `https://home.chpc.utah.edu/~u0816744/TIMPS/`

Schiro, K. A., F. Ahmed, S. E. Giangrande, and J. D. Neelin, 2018: Goamazon2014/5 campaign points to deep-inflow approach to deep convection across scales. *Proceedings of the National Academy of Sciences*, **115**, 4577–4582.

Schiro, K. A. and J. D. Neelin, 2019: Deep convective organization, moisture vertical structure, and convective transition using deep-inflow mixing. *Journal of the Atmospheric Sciences*, **76**, 965–987.

Schumacher, C., R. A. Houze Jr, and I. Kraucunas, 2004: The tropical dynamical response to latent heating estimates derived from the trmm precipitation radar. *Journal of the Atmospheric Sciences*, **61**, 1341–1358.

Schumacher, R. S. and K. L. Rasmussen, 2020: The formation, character and changing nature of mesoscale convective systems. *Nature Reviews Earth & Environment*, **1**, 300–314.

Sessions, S. L., S. Sentić, and D. J. Raymond, 2019: Balanced dynamics and moisture quasi-equilibrium in dynamo convection. *Journal of the Atmospheric Sciences*, **76**, 2781–2799.

Skok, G., J. Bacmeister, and J. Tribbia, 2013: Analysis of tropical cyclone precipitation using an object-based algorithm. *Journal of Climate*, **26**, 2563–2579.

Sobel, A., S. Wang, and D. Kim, 2014: Moist static energy budget of the mjo during dynamo. *Journal of the Atmospheric Sciences*, **71**, 4276–4291.

Stephens, G. L., D. G. Vane, S. Tanelli, E. Im, S. Durden, M. Rokey, D. Reinke, P. Partain, G. G. Mace, R. Austin, et al., 2008: Cloudsat mission: Performance and early science after the first year of operation. *Journal of Geophysical Research: Atmospheres*, **113**.

Vitart, F., R. Emerton, M. Rodwell, M. Balmaseda, T. Haiden, S. Johnson, et al., 2022: Investigating biases in the representation of the pacific sub-tropical jet stream and associated teleconnections (a ugrow sub-project). *ECMWF Technical Memorandum, 888*, 24.

Winker, D., J. Pelon, J. Coakley Jr, S. Ackerman, R. Charlson, P. Colarco, P. Flamant, Q. Fu, R. Hoff, C. Kittaka, et al., 2010: The calipso mission: A global 3d view of aerosols and clouds. *Bulletin of the American Meteorological Society*, **91**, 1211–1230.

Wolding, B., J. Dias, G. Kiladis, F. Ahmed, S. W. Powell, E. Maloney, and M. Branson, 2020: Interactions between moisture and tropical convection. part i: The coevolution of moisture and convection. *Journal of the Atmospheric Sciences*, **77**, 1783–1799.

Wolding, B., S. W. Powell, F. Ahmed, J. Dias, M. Gehne, G. Kiladis, and J. D. Neelin, 2022: Tropical thermodynamic–convection coupling in observations and reanalyses. *Journal of the Atmospheric Sciences*, **79**, 1781–1803.

Wolding, B. O., E. D. Maloney, and M. Branson, 2016: Vertically resolved weak temperature gradient analysis of the m adden-j ulian o scillation in sp-cesm. *Journal of Advances in Modeling Earth Systems*, **8**, 1586–1619.

Woodley, W. L., C. G. Griffith, J. S. Griffin, and S. C. Stromatt, 1980: The inference of gate convective rainfall from sms-1 imagery. *Journal of Applied Meteorology and Climatology*, **19**, 388–408.

Xin, Y., N. Lu, H. Jiang, Y. Liu, and L. Yao, 2021: Performance of era5 reanalysis precipitation products in the guangdong-hong kong-macao greater bay area, china. *Journal of Hydrology*, **602**, 126791.

Yang, G.-Y. and J. Slingo, 2001: The diurnal cycle in the tropics. *Monthly Weather Review*, **129**, 784–801.

Zipser, E. J., 2003: Some views on "hot towers" after 50 years of tropical field programs and two years of trmm data. *Meteorological Monographs*, **29**, 49–58.